Planta (2018) 247:69–97
https://doi.org/10.1007/s00425-017-2768-7

ORIGINAL ARTICLE

Comparative physiological and proteomic analyses reveal different adaptive strategies by *Cymbidium sinense* and *C. tracyanum* to drought

Jia-Wei Li[1,2,4] · Xiao-Dong Chen[5] · Xiang-Yang Hu[3] · Lan Ma[1,2] · Shi-Bao Zhang[1,2]

Received: 26 June 2017 / Accepted: 28 August 2017 / Published online: 4 September 2017

Abstract

Main conclusion **A terrestrial orchid, *Cymbidium sinense* appears to utilizes "remedy strategy", while an epiphytic orchid, *C. tracyanum*, employs a "precaution strategy" to drought stress based on morphological, physiological and proteomic analysis.**

Drought condition influences plant growth and productivity. Although the mechanism by which plants adapt to this abiotic stress has been studied extensively, the water-adaptive strategies of epiphytes grown in water-limited habitats remain undefined. Here, root and leaf anatomies, dynamic changes in physiological and proteomic responses during periods of drought stress and recovery studied in an epiphytic orchid (*Cymbidium tracyanum*) and a terrestrial orchid (*C. sinense*) to investigate their strategies for coping with drought. Compared with *C. sinense*, *C. tracyanum* showed stronger drought-resistant adaptive characteristics to drought because its leaves had more negative water potential at turgor loss point and roots had higher proportion of velamen radicum thickness. Although both species demonstrated quick recovery of photosynthesis after stress treatment, they differed in physiological and proteomic responses. We detected and functionally characterized 103 differentially expressed proteins in *C. sinense* and 104 proteins in *C. tracyanum*. These proteins were mainly involved in carbon and energy metabolism, photosynthesis, and defense responses. The up-regulated expression of plastid fibrillin may have contributed to the marked accumulation of jasmonates only in stressed *C. sinense*, while ferredoxin-NADP reductase up-regulation was only found in *C. tracyanum* which possibly related to the stimulation of cyclic electron flow that is linked with photoprotection. These physiological and proteomic performances suggest distinct adaptive strategies to drought stress between *C. sinense* (remedy strategy) and *C. tracyanum* (precaution strategy). Our findings may help improve our understanding about the ecological adaptation of epiphytic orchids.

Keywords Drought adaption · Proteomic analysis · Orchid · Epiphyte · Terrestrial species

Abbreviations

A_n	Net photosynthesis
g_s	Stomatal conductance
Ψ_{MD}	Midday leaf water content
F_v/F_m	Maximum quantum yield of PSII after dark adaptation overnight
P_m	Maximum photo-oxidizable P700
CEF	Cyclic electron flow

Electronic supplementary material The online version of this article (doi:10.1007/s00425-017-2768-7) contains supplementary material, which is available to authorized users.

✉ Shi-Bao Zhang
sbzhang@mail.kib.ac.cn

1 Key Laboratory for Economic Plants and Biotechnology, Kunming Institute of Botany, Chinese Academy of Sciences, 132 Lanhei Road, Kunming 650201, Yunnan, China

2 Yunnan Key Laboratory for Wild Plant Resources, Kunming 650201, China

3 College of Life Science, Shanghai University, Shanghai 200444, China

4 College of Life Science, University of Chinese Academy of Sciences, Beijing 100049, China

5 School of Environmental and Biological Engineering, Nanjing University of Science and Technology, Nanjing 210094, China

JA Jasmonates
ABA Abscisic acid

Introduction

Epiphytes are an important component of tropical and subtropical flora, and are especially rich within Orchidaceae (Zotz and Bader 2009). Both epiphytic and terrestrial life forms occur in the genus *Cymbidium* (Orchidaceae), which is distributed in tropical and subtropical Asia, and in northern Australia. Approximately 70% of the members within *Cymbidium* grow on trees (Zhang et al. 2001; Motomura et al. 2008). Numerous species in *Cymbidium* have long been cultivated as desirable ornamental plants worldwide. Some of them are now endangered in wild due to the destruction of natural habitats and climate change (Luo et al. 2002; Liu et al. 2009). Therefore, studying the adaptive mechanisms by which epiphytic and terrestrial *Cymbidium* species adapt to abiotic stress is beneficial for their utilization and conservation, and can improve our understanding of ecological strategy in orchids.

Because of their divergent life forms, closely related species may develop different mechanisms for adapting to their habitats (Zhang et al. 2016). Compared with terrestrial environments, epiphytic sites are usually characterized by restricted capacity to store available water and nutrients, as well as extreme fluctuations in light and temperature (Théry 2001). Among these abiotic factors, water is arguably the most limiting for the growth of vascular epiphytes (Zotz and Hietz 2001). However, the physiological and proteomic mechanisms that epiphytic orchids utilize under drought stress have remained undefined.

Plants optimize their morphology, physiology and metabolic processes at organ and cellular levels to cope with drought stress. The strategies for drought resistance include avoidance and tolerance, with the former being achieved via enhanced water uptake and reduced water loss (Chaves et al. 2002; Price et al. 2002). An adaptive structure for drought avoidance is velamen radicum, which may be important for maintaining the water balance in epiphytic orchids. This unique dead structure occurs on the root surface of most epiphytic orchids, acting as a sponge to absorb water within seconds during and immediately after a rain fall (Zotz and Tyree 1996; Zotz and Winkler 2013). We previously reported that epiphytic orchids have higher values for leaf mass per unit area, leaf thickness, epidermal thickness, saturated water content and the time required to dry saturated leaves to 70% relative water content. This indicated that ability to avoid drought of epiphytes is greater than terrestrial species (Zhang et al. 2015).

The well-known mechanisms for strategies of drought tolerance include the biosynthesis/de-conjugation of abscisic acid (ABA) and its signaling pathways, which lead to stomatal closure. Other tolerance mechanisms are mediated through osmotic adjustments, various secondary messengers, and transcriptional/post-transcriptional regulation that activates various drought-related genes (Reddy et al. 2004; Golldack et al. 2014). However, the entire process is more complex. For example, ABA is not the only phytohormone involved in drought stress response, and much evidence has been found of cross-talk between it and other phytohormones, such as jasmonates (JA) (Wilkinson et al. 2012). Furthermore, plants can be divided into two categories—isohydric or anisohydric—according to their stomatal regulation of water status (Tardieu and Simonneau 1998). Isohydric plants show reduced stomatal conductance when the soil water potential (Ψ_{soil}) decreases and atmospheric conditions are dry, making them able to maintain a relatively constant midday leaf water potential (Ψ_{leaf}) regardless of drought conditions. In contrast, anisohydric species allow midday Ψ_{leaf} to decline as Ψ_{soil} declines. For *C. sinense*, the transportation rate and stomatal resistance are more drought-sensitive than leaf water content, leaf water potential and chlorophyll content (Pan et al. 1993). This suggests that this species relies upon isohydric regulation of stomata. Photoprotection of photosystem II (PSII) and photosystem I (PSI) is another important process in the drought response. We have previously determined that, under strong irradiance or chilling stress, the activities of PSII and PSI are more sensitive in *C. sinense* than in *C. tracyanum*, and that stimulation of cyclic electron flow (CEF) may be a primary photoprotective mechanism in the latter species (Kuang and Zhang 2015; Li and Zhang 2016). Therefore, because of the complexity of mechanisms in drought response, further studies should focus on the physiological-, biochemical- and molecular-based aspects of the divergent life forms displayed among species of *Cymbidium.*

Although the molecular mechanisms for drought adaptations are now better understood (Yordanov et al. 2000; Shinozaki and Yamaguchi-Shinozaki 2007; Manavalan et al. 2009), investigating those mechanisms in members of Orchidaceae are more challenging because of their large genome size, low transformation efficiency, extended regeneration period, and long life cycle (Hossain et al. 2013). However, with the development of the proteomics technologies that have enabled more holistic studies of a wider range of plant species (Hajheidari et al. 2005; Bonhomme et al. 2009; Fulda et al. 2011), researchers can now examine strategies for drought adaptation in *Cymbidium* at cell, tissue and organic levels.

In the present study, we investigated the mechanisms and strategies underlying the responses by an epiphytic orchid (*C. tracyanum*) and a terrestrial orchid (*C. sinense*) to gradually anabatic drought stress and consequent water recovery by applying physiological and comparative proteomics. By

characterizing the adaptive mechanisms of the two species, we may ultimately be able to improve their utilization and conservation.

Materials and methods

Plant materials

We studied two species in *Cymbidium* to compare differences in the adaptive strategies by terrestrial and epiphytic plants to drought. *C. sinense* is a typical terrestrial orchid that always occurs on forest floors or in well-drained, shaded thickets in subtropical and tropical forests of southeastern China at elevations of 300–1500 m. In contrast, *C. tracyanum* is an epiphytic orchid that always grows on tree trunks in the subtropical forests of southwestern China at 1200–2000 m. To minimize the potential effect of developmental differences on our experimental results, we selected 30 mature individuals of fairly uniform size for each species. They were planted in the plastic pots containing bark mixtures, and placed in a greenhouse at the Kunming Institute of Botany, Kunming, China. Their growing conditions included an air temperature of 18–24 °C, relative humidity (RH) of 50–70, and 20% full sunlight. The plants were watered to maintain soil relative water content (RWC) of 65–75% before experimental treatments began. The soil RWC was defined by weighing individual pots, and was calculated as: (initial weight − final weight)/initial weight × 100.

Drought treatments

We investigated the response of *C. sinense* and *C. tracyanum* to gradually anabatic drought stress and water recovery. Before treatment, records were made of leaf morphology, root anatomy, gas exchange, chlorophyll fluorescence, midday leaf water content (Ψ_{MD}), concentrations of JA and ABA, activity of antioxidant enzymes catalase (CAT, EC1.11.1.6) and superoxide dismutase (SOD, EC1.15.1.1), and the concentrations of nonstructural carbohydrate in samples from each species. The leaf materials for proteomic analysis were frozen in liquid nitrogen and stored in −80 °C. Half of the plants for each species were arranged in a completely randomized design and watered to maintain soil RWC of 65–75% as the well-watered control treatment, and irrigation was halted for the other half to induce different degrees of drought stress. When the soil RWC values had declined to 40–45, 20–25, 10–15 and 5–10%, the parameters mentioned above were measured and leaf materials were collected from both species for proteomic analysis. After these drought treatments were completed, the soil RWC of those stressed plants was recovered to 60–75% by rewatering. During this phase of recovery, the gas exchange was measured daily until the values for stomatal conductance (g_s) and net photosynthesis (A_n) returned to the level recorded before drought treatment began. Following this 3-day recovery period, those parameters were again measured and leaf materials were collected.

Examination of root anatomy and leaf morphology

For each species, eight fresh mature roots were collected from individual plants. Transverse sections were examined and photographed with a digital camera mounted on a Leica DM2500 microscope (Leica Microsystems Vertrieb GmbH, Wetzlar, Germany). Photographs at 1.6× magnification were used to measure the ratio of velamen thickness to root semi-diameter with the Image J program, while the photographs at 10× magnification were used to observe the xylem conduits diameter (XCD) and the number of xylem conduits (NXC) in the roots.

Values for RWC and saturated water content (SWC) were calculated according to the method of Ogburn and Edwards (2012). The time needed to dry a saturated leaf to 70% RWC (T_{70}) was measured as described by Hao et al. (2010). Pressure–volume (*P–V*) curves were acquired using a WP4C Dewpoint Potentia Meter (Decagon, Pullman, WA, USA), based on the method of Ogburn and Edwards (2012). Water relations parameters derived from *P–V* curves included osmotic potential at full turgor (Π_o), water potential at turgor loss point (Ψ_{TLP}), relative water content at turgor loss point (RWC_{TLP}), volumetric elastic modulus (ε), capacitance before turgor loss (C_{FT}), and capacitance after turgor loss (C_{TLP}) (Tyree and Hammel 1972; Ogburn and Edwards 2012).

Measurements of gas exchange and chlorophyll fluorescence

The Li-6400 open gas exchange system (Li-Cor Inc., Lincoln, NE, USA) was used to determine the A_n and g_s from six mature leaves of each species. During this monitoring period, the RH was 60% and the air temperature was 22 °C, the CO_2 concentration was maintained at 400 μmol mol^{-1}. All measurements were made from 09:00 to 11:30 when CO_2 uptake was maximal.

The in vivo chlorophyll fluorescence of PSII and P700 redox state were measured with Dual PAM-100 (Heinz Walz, Effeltrich, Germany) that was connected to a computer with control software. The following parameters were examined: minimum fluorescence (F_0), maximum fluorescence (F_m), minimum fluorescence in light-adapted state (F'_o), the maximum quantum yield of PSII after dark adaptation overnight (F_v/F_m), and the effective quantum yield of PSII [Y(II)] (Kramer et al. 2004). Saturation pulses (10,000 μmol m^{-2} s^{-1}) were applied for assessing P700

parameters. Maximum photo-oxidizable P700 (P_m) was determined by applying a saturation pulse after pre-illumination with far-red light. Afterward the maximum change in P700 in a given light state (P'_m), the photochemical quantum yield of PSI [Y(I)] were calculated (Tikkanen et al. 2014). The value for Y(NA) represented the fraction of overall P700 that could not be oxidized by a saturation pulse in a given state due to a lack of acceptors, was calculated as $(P_m - P'_m)/P_m$. We estimated cyclic electron flow around PSI (CEF) as the difference in electron flow between PSI and PSII (Miyake et al. 2005).

Analysis of JA and ABA accumulation

After the leaf tissue was ground in fine power under liquid nitrogen, approximately 200 mg of each sample was collected in centrifugal tube. 1 mL of ethyl acetate was spiked with 200 ng of D_2-JA and 40 ng of D_4-ABA which was used as the internal standards for JA and ABA, was added to each crushed sample, respectively. The samples were then vortexed for 10 min. After centrifugation at 13,000*g* for 10 min at 4 °C, the supernatants were transferred to fresh 2-mL tubes. Each sample was re-extracted with 0.5 mL of ethyl acetate without internal standard. The supernatants were combined and then evaporated to dryness on a vacuum concentrator (Eppendorf, Hamburg, Germany). Each residue was re-suspended in 0.5 mL of 70% methanol (v/v), vortexed for 10 min, and centrifuged at 13,000*g* for 10 min at 4 °C to clarify phases. The supernatants were pipetted to glass vials and then analyzed by HPLC–MS/MS (high pressure liquid chromatography–mass spectrometry; LCMS-8040 system, Shimadzu, Kyoto, Japan). Measurements were conducted on a 1200 L LC–MS (Varian, Palo Alto, CA, USA). At a flow rate of 0.1 mL min^{-1}, 15 mL of each sample was injected onto a Pursuit C8 column (3 m, 150 × 2 mm; Varian). A mobile phase comprising solvent A (0.05% formic acid) and solvent B (0.05% formic acid in methanol) was used in a gradient mode for separation.

Analyses of total soluble sugars and starch

Approximately 0.1 g of dried leaves was put into a 10-mL centrifuge tube, and 5 mL of 80% ethanol was added. This mixture was incubated in an 80 °C water bath for 30 min, and then centrifuged at 4000*g* for 15 min. The concentration of total sugars was determined with a UV–visible spectrophotometer (UV-2500; Shimadzu, Kyoto, Japan) at 620 nm by the anthrone method (Seifter et al. 1949), and was calculated on a dry matter basis (% d.m.). Starch in the residue was released in 2 mL of distilled water for 15 min in a boiling water bath, and the concentration was measured with the UV–visible spectrophotometer 620 nm, using anthrone reagent. It was calculated by multiplying the glucose concentrations by a conversion factor of 0.9 (Li et al. 2008).

Monitoring the activities of antioxidant enzyme activity

Approximately 0.3 g of leaf collected from each sample was homogenized in 5 mL of 50 mM sodium phosphate (pH 7.0) buffer containing 1 mM EDTA, 1 mM dithiothreitol (DTT), 1 mM glutathione, 5 mM $MgCl_2.6H_2O$, 1% (w/v) PVP-40, and 20% (v/v) glycerin. The homogenates were centrifuged at 12,000*g* for 15 min at 4 °C, and the concentration of total soluble protein in the supernatants was measured by the Bradford method (Kruger 1994). Activity of CAT and SOD, activities were determined as the previously described (Nakano and Asada 1981; Jiang and Zhang 2001).

Protein extraction and two-dimensional gel electrophoresis

Protein extraction and two-dimensional electrophoretic (2DE) separation were performed according to a reported method with minor modifications (Yang et al. 2012; Li et al. 2014). Approximately 10 g of the leaf sample was ground in liquid nitrogen. Total soluble protein was extracted with 10% (w/v) TCA and 1% (w/v) DTT. The homogenates were maintained at −20 °C for 4 h, and then centrifuged at 25,000*g* for 30 min at 4 °C. The resultant pellets were washed with acetone containing 1% (w/v) DTT at −20 °C for 1 h, and then centrifuged. The final pellets were vacuum-dried and then dissolved in 8 M urea, 20 mM DTT, 4% (w/v) CHAPS, and 2% (w/v) ampholyte (pH 3–10). Samples in the ampholyte were vortexed thoroughly for 1 h at room temperature and then centrifuged at 25,000*g* for 20 min at 20 °C. Those supernatants were collected for 2DE experiment, and each experiment was repeated three times.

In-gel digestion, MALDI-TOF/TOF analysis and database search

Protein spots that showed significant changes in expression in parallel with changes in water status were excised manually from colloidal CBB-stained 2-DE gels. After the proteins were digested with trypsin mass spectrometry analyses were conducted using a MALDI-TOF/TOF mass spectrometer 4800-plus Proteomics Analyzer (Applied Biosystems, Farmington, MA, USA). The primary and secondary MS data were transferred to Excel files and used as inputs to search against an NCBI non-redundant database. This search was restricted to viridiplantae (green plants) using the MASCOT search engine.

Statistical analysis

Our statistical analyses were performed with SPSS 16.0. All data were subjected to analysis of variance (ANOVA), and Tukey's multiple comparison tests was used at the level of $\alpha = 0.05$ level to determine whether significant differences existed between treatments.

Results

Differences in water-related traits between *C. sinense* and *C. tracyanum*

The cross-sections of roots from *C. sinense* and *C. tracyanum* were anatomically similar, with showing a multilayer velamen radicum, epidermis, cortex, and pericycle (Fig. 1). However, *C. tracyanum* had higher ratios of velamen radicum thickness to root semi-diameter and xylem conduit diameter (Supplement Information Table S1).

Compared with *C. sinense*, the Ψ_{TLP} value for *C. tracyanum* was more negative, its RWC_{TLP} was lower, and its T_{70} was longer (Table S1). These findings suggested that leaf water was better conserved in *C. tracyanum* than in *C. sinense*.

Physiological responses of *C. sinense* and *C. tracyanum* to drought

Under well-watered control conditions, the values were significantly higher for A_n ($p < 0.01$) and g_s ($p < 0.05$) in *C. tracyanum* than in *C. sinense*. However, the levels of both parameters were decreased for both species when the drought stress was intensified. Under both stress and recovery conditions, values for Ψ_{MD} did not change significantly (Fig. 2a). Nevertheless, A_n remained significantly higher

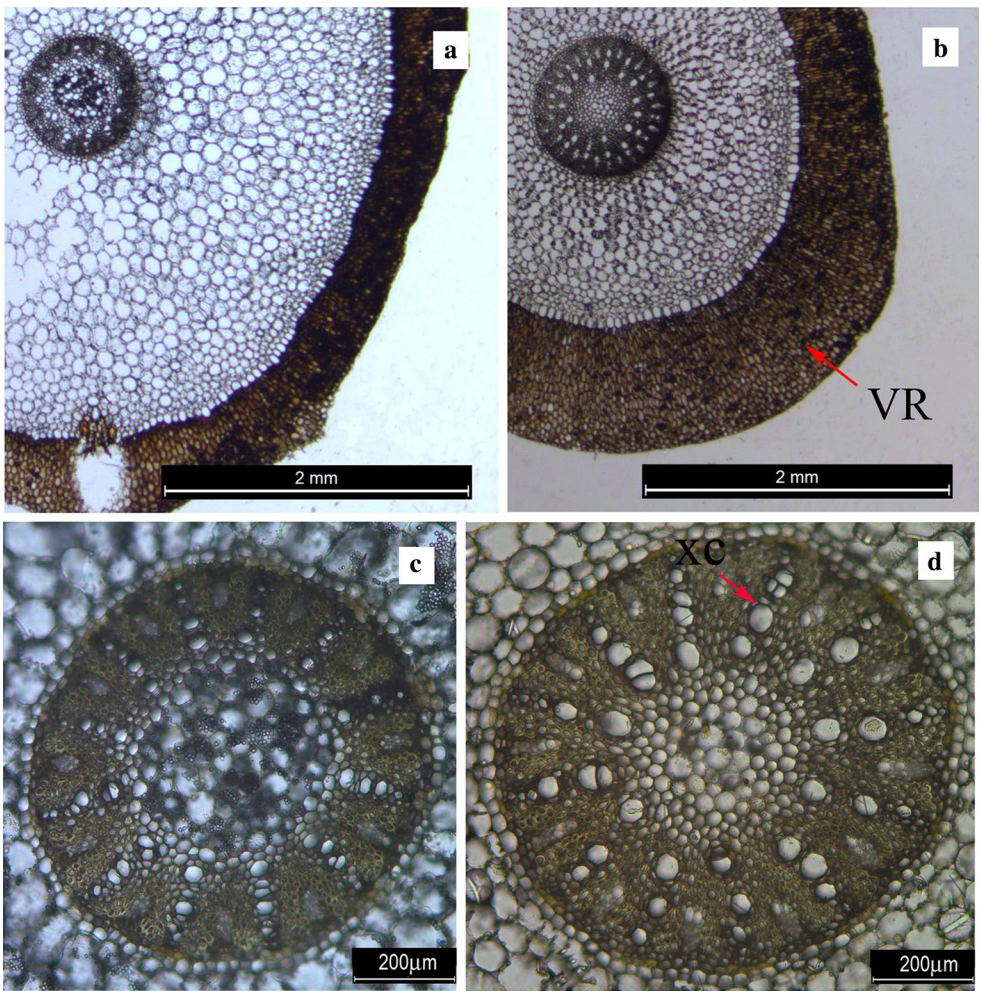

Fig. 1 Anatomical observations of organs from *Cymbidium sinense* and *C. tracyanum*. **a** Root cross section from *C. sinense*; **b** root cross section from *C. tracyanum*; **c** pericycle cross section from *C. sinense*; **d** pericycle cross section from *C. tracyanum*. *VR* velamen radicum, *XC* xylem conduits

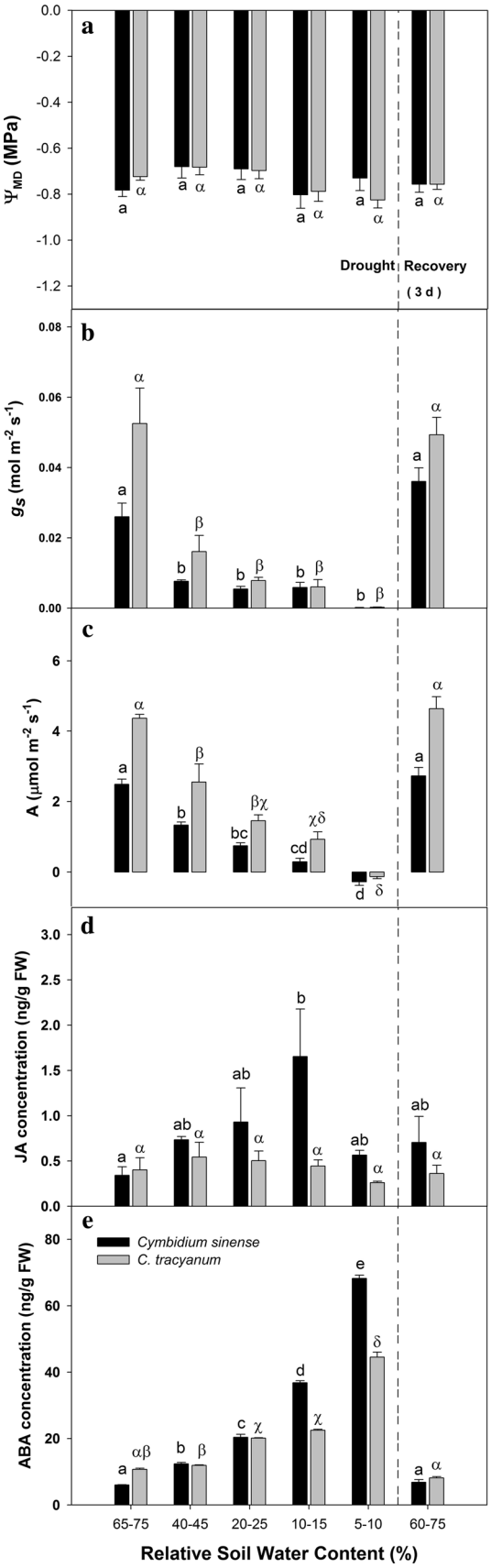

Fig. 2 Changes in midday leaf water potential (Ψ_{MD}) (**a**); stomatal conductance (g_s) (**b**); net photosynthesis (A_n) (**c**); concentrations of jasmonic acids (JA) (**d**); and abscisic acid (ABA) (**e**) in *Cymbidium sinense* and *C. tracyanum* plants during drought-stress treatment. *Each vertical bar* represents mean ± SE for five measurements from individual plants. *Different letters* above *bars* indicate significant differences in each parameter between treatments ($p < 0.05$, based on ANOVA, followed by Tukey's post hoc tests for comparison)

($p < 0.05$) in *C. tracyanum* than in *C. sinense* after the soil RWC dropped to 10–15% (Fig. 2b, c). In parallel with the decline in g_s, ABA concentration in both species increased gradually as soil RWC decreased. Although the ABA concentration was higher in *C. tracyanum* than in *C. sinense* under control conditions, it was lower when the soil RWC dropped to 10–15% ($p < 0.01$) (Fig. 2e). JA concentration did not significantly change in *C. tracyanum* during drought treatment, but dramatically increased in *C. sinense* when soil RWC dropped to 10–15% (Fig. 2d). After the plants were re-watered for 3 days, the values for A_n, g_s, ABA and JA concentration recovered quickly within 3 days.

During both the drought period and 3 days of recovery, neither F_v/F_m nor P_m changed significantly (Fig. 3a). However, CEF_{max} was more strongly stimulated by drought in *C. tracyanum* than in *C. sinense* during treatment (Fig. 3b). The value for $Y(NA)_{233}$ significantly increased in *C. sinense* when soil RWC dropped to 5–10% at a photon flux density of 233 mol m^{-2} s^{-1}. In contrast, no remarkable change was observed in *C. tracyanum*. Under both stress and recovery conditions, $Y(NA)_{233}$ values were higher in the former than the latter (Fig. 3c).

Before the drought treatments began, sugar concentration was higher in *C. tracyanum* than in *C. sinense* ($p < 0.05$), starch concentration was not significantly different between species before treatment, but decreased dramatically in *C. sinense* when soil RWC dropped to 10–15%, and did not recover after 3 days of re-watering (Fig. 4a, b). Finally, under both stress and recovery conditions, the activity did not significantly altered for either CAT (Fig. 4c) or SOD (Fig. 4d).

Leaf protein profiles for *C. sinense* and *C. tracyanum*

The leaf proteome was analyzed under different soil water status, i.e., control (65–75% RWC) drought stress (40–45, 20–25, 10–15, or 5–10%), and 3-day water recovery (60–75%). Those experimental conditions led to significant variations in the protein yields for both species. Out of the 410–460 protein spots detected 132 (*C. sinense*) and 139 (*C. tracyanum*) significantly changed in response to stress ($p < 0.05$). When compared with the samples from the control plants, all of these proteins showed increased abundance (>1.5) or decreased abundance (<−1.5) under stress and recovery conditions. Among them 103 proteins from *C. sinense* and 104

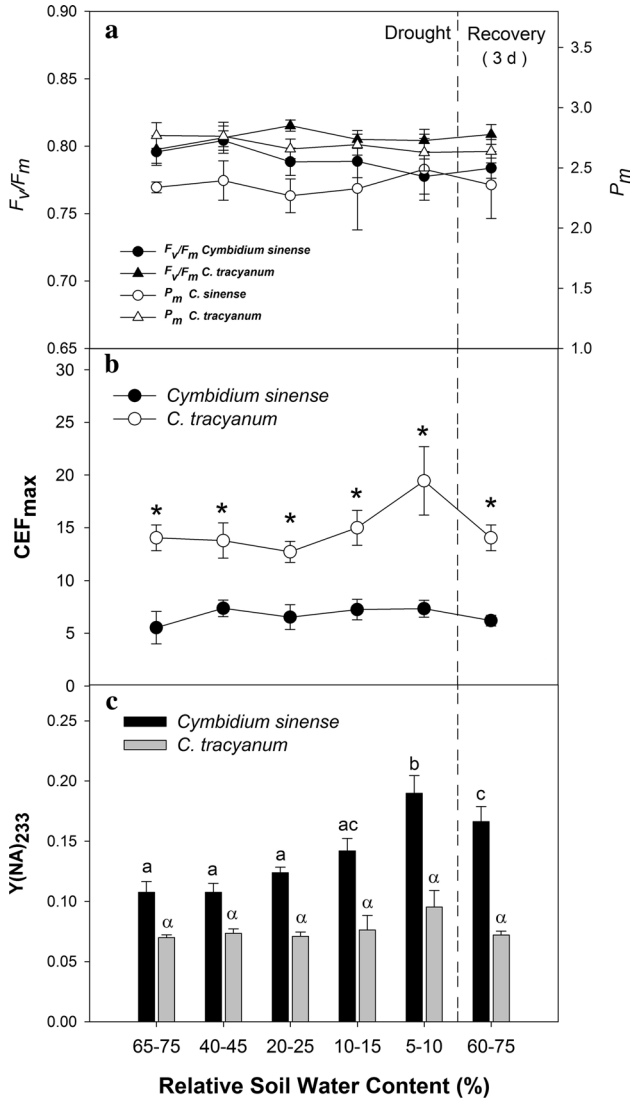

Fig. 3 Changes in maximum quantum yield of photosystem II after dark adaption (F_v/F_m) and maximum photo-oxidizable P700 (P_m) (**a**), maximum ratio of cyclic electron flow around PSI (CEF_{max}) (**b**) and PSI acceptor side limitation at 233 µmol photons m^{-2} s^{-1} [$Y(NA)_{233}$] (**c**) for *Cymbidium sinense* and *C. tracyanum* plants during drought-stress treatment. *Each vertical bar* represents mean ± SE for four measurements from individual plants. *Different letters* above *bars* indicate significant differences in each parameter between treatments ($p < 0.05$, based on ANOVA, followed by Tukey's post hoc tests for comparison). Statistical differences (p values) between the two species at each treatment were determined with independent-sample t tests. ($^{ns}p > 0.05$; $^{*}p < 0.05$; $^{**}p < 0.01$, $^{***}p < 0.001$)

proteins from *C. tracyanum* were identified by MALDI-TOF/TOF and corresponded to eight putative classes of biological functions (Fig. 5). For *C. sinense*, the proteins related to carbon and energy metabolism (28.2%), defense responses (16.5%) and photosynthesis (13.6%) accounted for 58.3% of the total proteins; whereas for *C. tracyanum*, proteins related to carbon and energy metabolism (29.8%), photosynthesis (17.4%) and antioxidation (14.4%) accounted for 61.6% of all proteins. Other functions included protein kinase and phosphatase, cell structure and division, protein synthesis, degradation and refolding and transcriptional and signal factor (Fig. 6). The results of our Venn diagram analysis proved that more proteins were up-regulated rather than down-regulated as drought conditions were intensified (Fig. 7).

The expression levels of several proteins involved in photosynthesis were altered with water status. The expression of oxygen-evolving enhancer protein (Table 1; spot T66, spot T67, spot T69) in *C. tracyanum* was up-regulated at soil RWC of 40–45, 20–25 and 10–15%, but was down-regulated for *C. sinense* (Table 1; spot S68, spot S94) when soil RWC dropped down to 40–45 and 10–15%, and the recovery. In *C. tracyanum*, the FtsH-like protein Pftf (Table 1; spot T17) was down-regulated as soil RWC decreased to 5–10%, but was recovered as the stress alleviated. The level of ferredoxin-NADP reductase (FNRs) was up-regulated during the stress period and recovery phase (Table 1; spot T55). However, the expression level of cytochrome b_6-f complex iron–sulfur subunit (Table 1; spot S99; spot T100) fluctuated in both species.

In the group of protein carbon and energy metabolism, the expression level of Rubisco activase was up-regulated under drought as well as recovery (Table 1; spot T41; spot T42, spot T49) in *C. tracyanum*, while for *C. sinense*, some Rubisco activase (Table 1; spot S33, spot S29, S35) was down-regulated during drought treatment and even recovery condition. Expression of phosphoglycolate phosphatase (Table 1; spot T70) was up-regulated in *C. tracyanum*, and the expression of fructose-bisphosphate aldolase (Table 1; spot S42) was significantly up-regulated (7.7- to 13.1-fold) in drought stress in *C. sinense*.

In the group of antioxidation, the expression level of CAT (Table 1; spot S19) was up-regulated at the beginning of the drought treatments, and down-regulated during recovery phase in *C. sinense*. The expression level of SOD (Table 1; spot T97, spot T101) was continuously up-regulated during the drought treatment period in *C. tracyanum*. Expression level of APX of *C. tracyanum* (Table 1; spot T77, spot T85) was up-regulated during the drought period. For *C. sinense*, the expression of chloroplast L-ascorbate peroxidase isoform (Table 1; spot S53) was up-regulated during water recovery.

The expression level of plastid fibrillin (Table 1, spot S84), a protein related to defense response, was up-regulated only in *C. sinense* when soil RWC dropped to 10–45%.

Discussion

Water-adaptive traits of *C. sinense* and *C. tracyanum*

When compared with *C. sinense*, *C. tracyanum* showed stronger adaptive characteristics of drought resistance. This

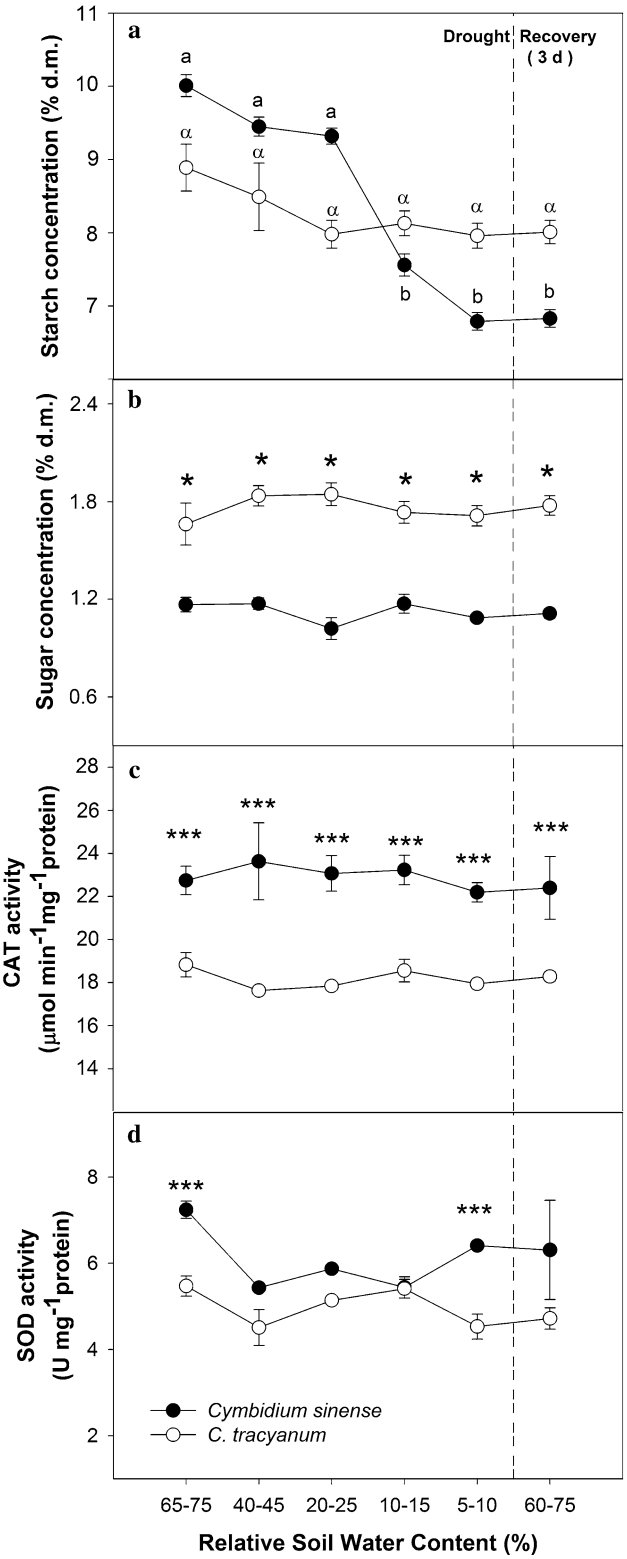

Fig. 4 Changes in starch concentration (**a**), sugar concentration (**b**), ▶ activities of antioxidant CAT (**c**) and SOD (**d**) for *Cymbidium sinense* and *C. tracyanum* during period of drought-stress. *Each vertical bar* represents mean ± SE for four measurements from individual plants. *Different letters* above *bars* indicate significant differences in each parameter between treatments ($p < 0.05$, based on ANOVA, followed by Tukey's post hoc tests for comparison). Statistical differences (p values) between the two species at each treatment were determined with independent-sample t tests. ($^{ns}p > 0.05$; $^{*}p < 0.05$; $^{**}p < 0.01$, $^{***}p < 0.001$)

is consistent with our earlier conclusion that epiphytes are more drought-resistant than terrestrial species in *Cymbidium* (Zhang et al. 2015). The velamen radicum has been studied extensively in Orchidaceae (Porembski and Barthlott 1988). Although it is more common in epiphytic orchids, it occurs in both epiphytic and terrestrial species of *Cymbidium* (Yukawa and Stern 2002). The most important role of velamen radicum appears to be the absorption of water and nutrients, but it also reduces water loss (Zotz and Winkler 2013; Benzing et al. 1982). Here, the epiphytic *C. tracyanum* had a higher radio of velamen thickness to root thickness, along with larger-diameter xylem conduits than those of the terrestrial *C. sinense*. This further indicated that *C. tracyanum* has a greater capacity to conserve water and avoid the negative effects of drought (Chaves et al. 2002).

The loss of cell turgor has an important impact on cellular structural integrity, metabolism and whole-plant performance (Brodribb et al. 2003; McDowell 2011). Thus, researchers use the parameter of leaf water potential at turgor loss to assess physiological drought tolerance. Plants with low Ψ_{TLP} tend to maintain more normal stomatal conductance, hydraulic conductance, photosynthetic gas exchange, and growth under drought stress (Blackman et al. 2010; McDowell 2011). We also noted that the Ψ_{TLP} of *C. tracyanum* was more negative than *C. sinense*, indicating that the former has greater capacity for drought tolerance.

Drought-induced stomatal closure in *C. sinense* and *C. tracyanum*

Values for g_s gradually decline in both species along with the stability of Ψ_{MD}. Anisohydric tree species tend to occupy more drought-prone habitats when compared with isohydric species, and xylem in the former is more resistant to negative water potential (McDowell et al. 2008; Klein 2014). Thus, stomatal regulation in our two tested species appears to be isohydric.

Although the two species utilize similar mechanisms for controlling stomatal activity, they differ somewhat in their regulatory processes. Under well-watered condition, g_s was significantly higher in *C. tracyanum* than in *C. sinense*, but no statistically significant difference in g_s was observed between species during the drought period. As a controlling factor of stomatal closure and positive response to drought stress (Mittler and Blumwald 2015), ABA concentrations increased faster and reached a higher level in *C. sinense* than in *C. tracyanum*, possibly showing that the stomatal

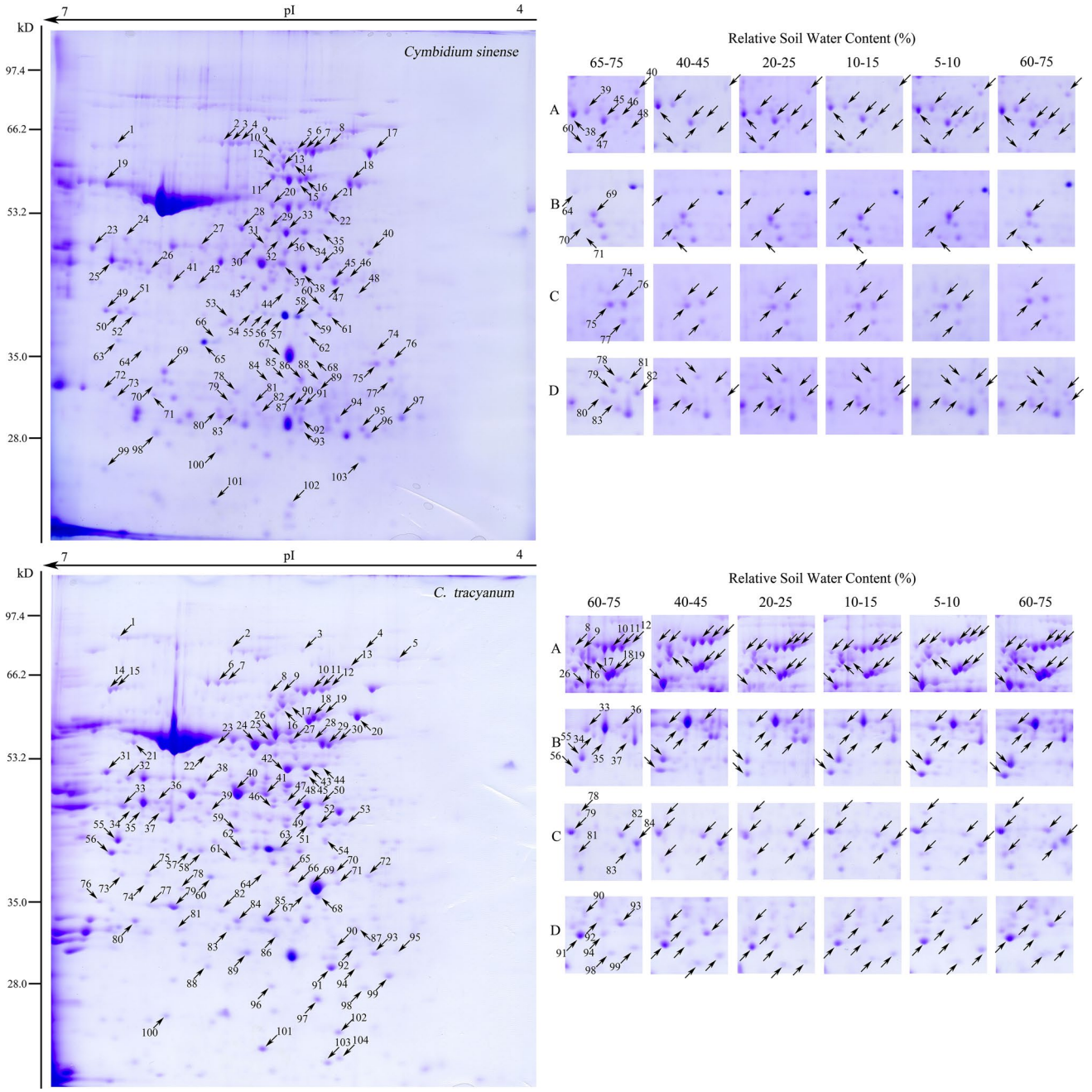

Fig. 5 Dynamic changes in protein spot abundance in *Cymbidium sinense* and *C. tracyanum* during drought-stress treatment. Plant samples were collected at different soil relative water content (65–75, 40–45, 20–25, 10–15, 5–10, 60–75%) and 1 mg of total protein was extracted and loaded into gels BR-20-stained 2-D gels of total protein. Enlarged windows from panel **a** showing spot changes in the representative gels from samples collected during drought-stress treatment

control is more flexible in the latter. In contrast, amount of ABA in *C. sinense* was perhaps remedied by improving the level of signals.

The phytohormone JA has also been proposed as an important signal for stomatal closure considering its accumulation and positive regulatory role in stomatal closure under drought stress (Suhita et al. 2004). Here, JA concentration in *C. sinense* was dramatically increased and was higher than in *C. tracyanum* when soil RWC dropped to 10–15%. This phenomenon might support the above-mentioned "remedy strategy". In *Arabidopsis*, plant fibrillin (FIB1-2) initiates the chloroplast stress-related biosynthesis of JA (Youssef et al. 2010). For *C. sinense*, the level of plastid fibrillin (Table 1; spot S84) was up-regulated when soil

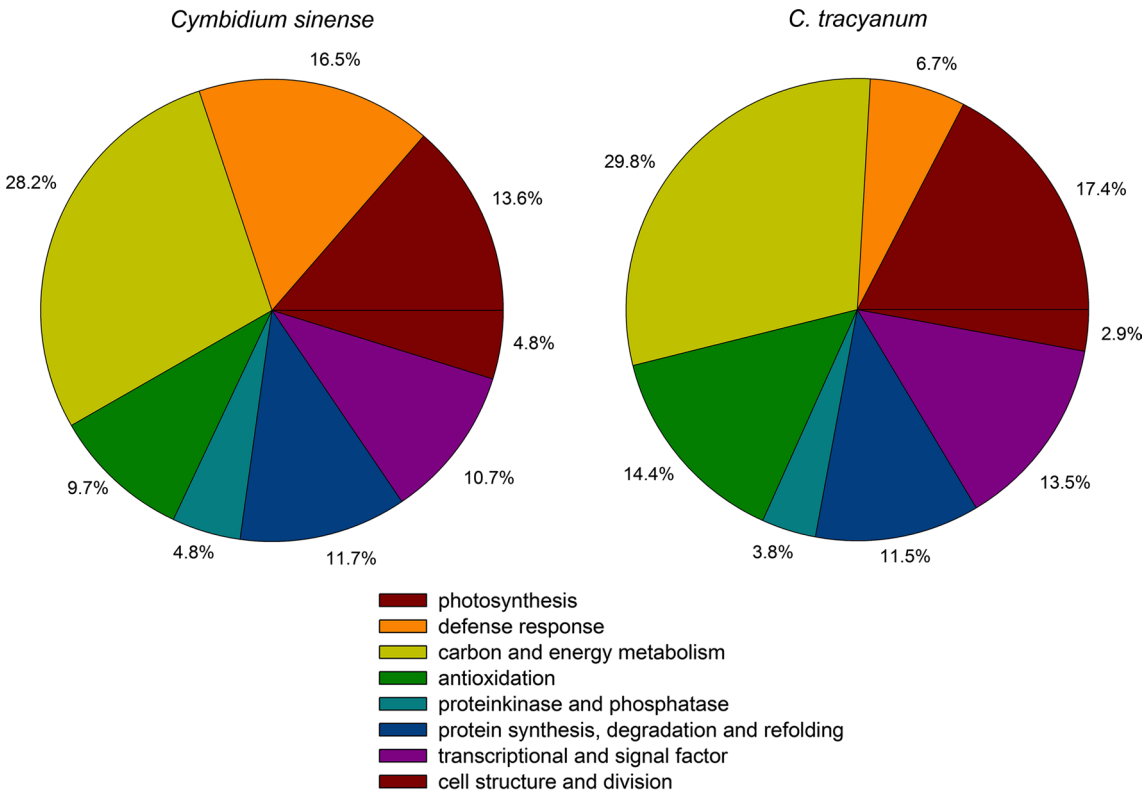

Fig. 6 Functional classification of proteins differentially expressed in *Cymbidium sinense* and *C. tracyanum* during drought-stress treatments

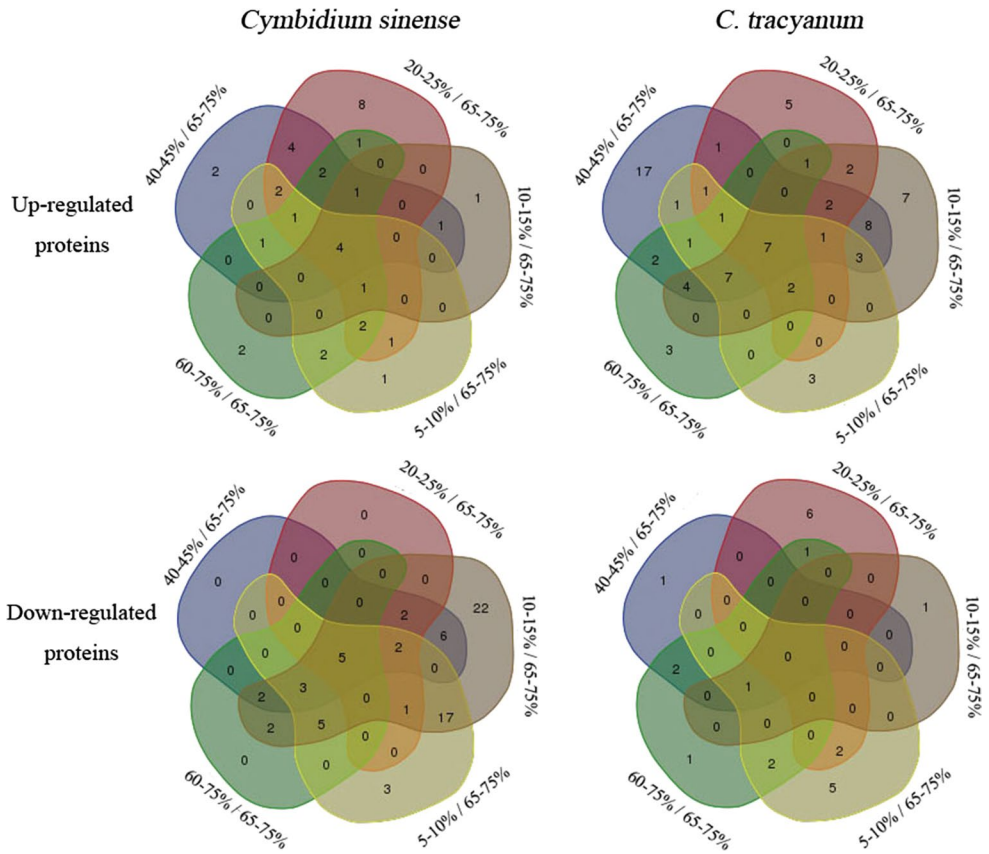

Fig. 7 Venn diagram of proteins differentially expressed during drought-stress treatment

Table 1 Identification of differentially-expressed proteins following treatment in leaves of *Cymbidium sinense* and *C. tracyanumas* analyzed by MALDI-MS/MS

Spot no.	Uniprot accession no.	Protein name	Species	Exp.Mw/pI	Theo. Mw/pI	Score	Coverage	Matched peptide	Radio				
									40–45%/65–75%	20–25%/65–75%	10–15%/65–75%	5–10%/65–75%	(Recovery)
	Photosynthesis												
S44	PHYB_ARATH	Phytochrome B	*Arabidopsis thaliana*	13.0/5.62	36.0/5.53	71	29.01	24	1.39	1.34	−2.01	−1.17	1.14
S58	A4S3P1_OSTLU	LHCII kinase	*Ostreococcus lucimarinus*	68.0/6.96	30.2/5.47	73	49.18	20	−1.56	1.30	−1.53	1.24	1.11
S67	A7LCN2_MORNI	Chloroplast photosynthetic water oxidation complex 33 kDa subunit	*Morus nigra*	28.5/5.48	24.5/5.68	236	67.92	10	−1.87	−1.69	−2.44	−1.29	−1.40
S68	T2DNJ8_PHAVU	Oxygen-evolving enhancer protein 1	*Phaseolus vulgaris*	35.2/6.08	24.4/5.38	136	62.31	12	−1.41	1.06	−1.59	1.18	−1.64
S75	CHRC2_ONCHC	Chromoplast-specific carotenoid-associated protein C2, chromoplastic	*Oncidium* hybrid cultivar	34.7/5.48	23.6/5.03	438	54.55	8	−1.23	−1.39	−1.76	−1.55	−1.18
S76	CHRC1_ONCHC	Chromoplast-specific carotenoid-associated protein C1, chromoplastic	*Oncidium* hybrid cultivar	34.7/5.33	23.7/4.93	464	62.70	9	−1.35	−1.37	−1.67	−1.48	−1.13
S77	B9GND3_POPTR	Phytoene dehydrogenase family protein	*Populus trichocarpa*	65.0/7.19	21.7/4.94	73	45.14	17	−1.16	−1.33	−1.83	−2.10	−1.40
S83	Q6Y0E5_VITVI	Chlorophyll *a/b* binding protein	*Vitis vinifera*	18.0/7.03	16.5/5.80	109	56.63	5	−1.52	−1.29	−3.43	−1.36	−1.93
S91	A0A0B2PBP0_GLYSO	Chlorophyll *a–b* binding protein CP26, chloroplastic	*Glycine soja*	30.9/6.34	18.6/5.45	163	31.60	5	−1.16	1.27	−1.57	−1.25	−1.19
S92	V9LU30_DENLA	Light harvesting chlorophyll *a/b*-binding protein 2-1	*Dendrocalamus latiflorus*	28.6/5.62	17.5/5.46	135	15.21	2	1.04	1.63	1.04	1.02	1.51
S94	Q9MAW2_BRUGY	Oxygen evolving enhancer protein 2	*Bruguiera gymnorhiza*	17.6/4.91	16.4/5.30	120	51.25	6	−1.64	−1.01	−2.35	−1.21	−1.21
S97	A0A072VAK2_MEDTR	Light-harvesting complex I chlorophyll *A/B*-binding protein	*Medicago truncatula*	25.9/4.96	17.6/4.88	85	33.33	6	−1.39	1.50	−1.53	−1.33	1.15
S98	A0A0B0MHC6_GOSAR	Chlorophyll *a–b* binding 6A, chloroplastic	*Gossypium arboreum*	27.0/6.22	15.6/6.31	347	44.53	5	−1.10	−1.06	−2.28	−1.25	−1.35
S99	A0A059BMK7_EUCGR	Cytochrome b6-f complex iron-sulfur subunit	*Eucalyptus grandis*	22.4/8.75	12.1/6.63	188	36.84	4	−1.14	−1.18	−2.05	−1.38	−1.22

Table 1 (continued)

Spot no.	Uniprot accession no.	Protein name	Species	Exp.Mw/pI	Theo. Mw/pI	Score	Coverage	Matched peptide	Radio				
									40–45%/65–75%	20–25%/65–75%	10–15%/65–75%	5–10%/65–75%	(Recovery)
	Defense response												
S1	D2E9R6_DACGL	Hsp organizing protein/stress-inducible protein	*Dactylis glomerata*	64.8/6.11	69.2/6.56	166	35.12	13	−1.10	−1.31	−2.01	−1.80	−1.35
S13	W9RHR9_9ROSA	ATP-dependent zinc metalloprotease FTSH 2	*Morus notabilis*	74.4/5.95	65.6/5.56	534	76.66	26	−1.06	−1.12	−1.82	−1.14	1.12
S14	B9DHR0_ARATH	AT2G30950 protein	*Arabidopsis thaliana*	74.2/6.00	66.1/5.52	544	53.67	19	−1.30	1.04	−2.22	−1.46	−1.38
S26	A9NVT9_PICSI	Malate dehydrogenase	*Picea sitchensis*	41.7/7.04	36.1/6.38	180	53.68	10	1.22	1.03	−1.77	−1.17	1.04
S36	H6U638_CYMEN	Actin	*Cymbidium ensifolium*	41.8/5.31	41.9/5.56	286	97.08	15	1.02	1.05	−2.08	−1.51	−1.33
S47	B6RCM0_TOBAC	Chilling-responsive protein	*Nicotiana tabacum*	35.7/4.86	34.8/5.21	145	23.44	2	−1.25	3.21	−1.40	−1.22	−1.30
S49	D3YJ40_9LAMI	Phenylcoumaran benzylic ether reductase-like protein	*Salvia fruticosa*	33.8/6.01	28.0/6.64	149	16.99	3	1.16	1.06	−1.37	−1.51	1.01
S50	A0A068ERY8_9ASPA	Isoflavone reductase-like protein	*Dendrobium catenatum*	34.2/5.67	27.9/6.55	130	32.69	5	1.38	1.26	1.02	1.76	1.53
S64	O04002_SOLTU	CDSP32 protein (chloroplast drought-induced stress protein of 32 kDa)	*Solanum tuberosum*	33.8/8.07	24.3/6.38	110	43.58	9	1.66	1.27	−1.92	−1.04	1.09
S60	QORL_ARATH	Quinone oxidoreductase-like protein At1g23740, chloroplastic	*Arabidopsis thaliana*	41.1/8.46	31.0/5.35	91	36.79	8	−1.95	1.12	−2.09	1.30	−1.54
S61	A0A067GEY3_CITSI	Lactoylglutathione lyase	*Citrus sinensis*	31.0/6.15	29.8/5.29	189	44.57	7	1.01	1.55	−1.67	1.31	−1.10
S79	Q4EWB8_AVIMR	Ferritin	*Avicennia marina*	29.2/5.73	18.7/5.88	102	33.33	6	−7.70	−5.70	−3.80	−3.71	−3.73
S57	G3JVJ6_FRAAN	ABA-, stress-and ripening-induced protein	*Fragaria ananassa*	21.0/6.03	30.1/5.55	65	52.08	2	−1.24	1.35	−1.85	1.13	1.08
S81	FRI1_TOBAC	Ferritin-1, chloroplastic	*Nicotiana tabacum*	28.5/5.70	18.7/5.74	138	48.61	8	−7.68	−3.70	−4.24	−2.18	−2.34
S84	G7I4U4_MEDTR	Plastid fibrillin	*Medicago truncatula*	29.8/6.91	20.7/5.66	118	32.25	7	1.57	1.50	1.57	1.21	1.45

Table 1 (continued)

Spot no.	Uniprot accession no.	Protein name	Species	Exp.Mw/pI	Theo. Mw/pI	Score	Coverage	Matched peptide	Radio				
									40–45%/65–75%	20–25%/65–75%	10–15%/65–75%	5–10%/65–75%	(Recovery)
S93	M0RNM6_MUSAM	Lactoylglutathione lyase	*Musa acuminata* subsp. *malaccensis*	26.4/6.97	16.3/5.46	219	84.12	13	−1.62	−1.12	−1.62	−1.18	−1.16
S101	Q53E26_TOBAC	Cytosolic class I small heat shock protein 3A	*Nicotiana tabacum*	14.0/5.80	11.9/6.04	105	86.29	7	−2.44	−1.03	−2.74	−2.60	−1.56
	Carbon, nitrogen and energy metabolism												
S2	Q8MG19_9LAMI	Ribulose 1,5-biphosphate carboxylase large subunit	*Sideritis montana*	51.0/6.46	72.9/5.96	93	49.12	18	1.38	−1.33	−1.69	−1.44	1.06
S3	TKTC_MAIZE	Transketolase, chloroplastic	*Zea mays*	73.3/5.47	73.0/5.91	76	16.59	10	1.33	1.00	−1.35	1.20	1.43
S6	Q9M6R1_MALDO	High molecular weight heat shock protein	*Malus domestica*	71.6/5.17	71.2/5.45	95	25.54	7	1.01	1.20	−1.94	−2.07	−1.14
S7	S8C6K2_9LAMI	Heat shock protein 70	*Genlisea aurea*	71.6/5.06	70.6/5.41	208	71.67	21	1.10	1.03	−2.29	−1.63	−1.09
S8	A0A0B2QKL2_GLYSO	Heat shock cognate 70 kDa protein	*Glycine soja*	71.1/5.14	71.4/5.23	261	72.60	24	−1.41	1.29	−2.30	−1.14	−1.55
S9	K7V6P0_MAIZE	Putative ATPase, V1 complex, subunit A protein	*Zea mays*	68.8/5.36	69.0/5.64	139	53.22	17	−1.38	−1.92	−2.64	−1.70	−1.42
S10	B6UH55_MAIZE	Vacuolar ATP synthase catalytic subunit A	*Zea mays*	68.7/5.30	67.1/5.66	94	32.05	13	−1.66	−1.59	−2.41	−2.22	−1.77
S12	A0A0B2RC62_GLYSO	2,3-Bisphosphoglycerate-independent phosphoglycerate mutase	*Glycine soja*	61.1/5.45	63.5/5.61	254	40.79	14	−1.58	−2.38	−2.79	−1.59	−2.28
S20	M9YUY4_9ASPA	ATP synthase subunit beta, chloroplastic	*Cymbidium mannii*	53.9/5.37	53.1/5.64	485	132.13	26	1.66	1.56	1.33	1.97	1.65
S21	M0RZE5_MUSAM	ATP synthase subunit beta	*Musa acuminata* subsp. *malaccensis*	45.3/5.35	53.8/5.31	437	81.15	15	1.04	1.46	−1.17	1.76	−1.24
S22	G7KNB8_MEDTR	Phosphopyruvate hydratase	*Medicago truncatula*	46.5/5.90	51.6/5.32	177	58.51	11	−1.16	1.09	−2.06	−1.69	−1.77
S23	R0HMD0_9BRAS	Fructose-bisphosphate aldolase	*Capsella rubella*	38.9/7.59	38.8/6.73	291	62.57	13	1.35	1.87	−1.28	1.07	1.22
S25	K4PDQ2_9ASPA	Glyceraldehyde-3-phosphate dehydrogenase	*Cymbidium faberi*	36.9/6.27	36.0/6.61	539	68.24	11	1.70	1.58	1.05	1.14	1.16

Table 1 (continued)

Spot no.	Uniprot accession no.	Protein name	Species	Exp.Mw/pI	Theo. Mw/pI	Score	Coverage	Matched peptide	Radio				
									40–45%/65–75%	20–25%/65–75%	10–15%/65–75%	5–10%/65–75%	(Recovery)
S28	RCAB_HORVU	Ribulose bisphosphate carboxylase/oxygenase activase B, chloroplastic	*Hordeum vulgare*	47.4/7.59	46.8/5.84	315	57.41	14	1.37	1.19	−1.81	−1.19	−1.13
S29	Q9AXG1_GOSHI	Ribulose-1,5-bisphosphate carboxylase/oxygenase activase 1	*Gossypium hirsutum*	48.2/5.54	46.6/5.67	287	60.27	14	1.00	−1.20	−2.51	−1.85	−1.91
S33	K7S704_GOSBA	Chloroplast ribulose bisphosphate carboxylase/oxygenase activase beta1	*Gossypium barbadense*	33.2/5.09	46.2/5.55	373	76.35	9	−1.54	−1.92	−2.33	−1.46	1.09
S35	C1K241_PLESU	Chloroplast ribulose-1,5-bisphosphate carboxylase/oxygenase activase	*Plectranthus scutellarioides*	47.7/8.16	46.7/5.35	305	49.54	10	−2.12	−1.40	−1.61	1.03	−1.42
S37	K7RYG4_GOSBA	Chloroplast ribulose bisphosphate carboxylase/oxygenase activase beta2	*Gossypium barbadense*	33.1/5.09	39.4/5.57	497	88.18	13	−1.15	−1.40	−1.94	−1.15	−1.40
S42	I1NJR7_ORYGL	Fructose-bisphosphate aldolase	*Oryza glaberrima*	42.2/8.81	34.2/6.09	274	56.70	11	13.05	9.99	7.67	8.62	11.98
S45	D7TMH3_VITVI	Putative uncharacterized protein	*Vitis vinifera*	42.9/5.95	35.5/5.26	336	58.78	12	−1.20	1.08	−1.56	−1.22	−1.21
S46	A8DUA7_MORAL	Chloroplast sedoheptulose-1,7-bisphosphatase	*Morus alba* var. *multicaulis*	42.8/6.06	35.9/5.19	135	31.63	7	−1.33	1.54	−1.42	1.10	1.20
S48	E5GC94_CUCME	Fructokinase	*Cucumis melo* subsp. *melo*	35.8/5.61	33.6/5.16	254	32.33	7	1.15	1.30	−1.27	−2.11	−1.26
S51	Q1XEL8_9LILI	Ribulose bisphosphate carboxylase large subunit	*Korthalsia cheb*	48.7/6.23	28.6/6.51	392	91.03	22	1.24	1.47	−1.37	1.36	1.25
S55	A0A0B2RVZ4_GLYSO	Xylulose kinase	*Glycine soja*	13.7/9.23	30.1/5.74	91	129.03	12	−1.08	1.95	1.31	1.32	−1.41
S63	A0A061DFL1_THECC	Gamma carbonic anhydrase 1, CA1	*Theobroma cacao*	29.7/6.32	24.0/6.59	132	76.75	10	1.99	2.07	1.20	−1.93	4.27
S70	I6RZD4_ERYCB	Putative NAD-dependent dehydrogenase 2	*Erythroxylum coca*	27.4/5.64	20.6/6.27	92	52.17	6	1.29	1.38	−1.66	−1.13	1.01
S78	TPIC_SECCE	Triosephosphate isomerase, chloroplastic	*Secale cereale*	32.0/6.00	19.8/5.85	282	44.63	8	−1.12	−1.03	−1.95	−1.11	−1.11

Table 1 (continued)

Spot no.	Uniprot accession no.	Protein name	Species	Exp.Mw/pI	Theo. Mw/pI	Score	Coverage	Matched peptide	Radio				
									40–45%/65–75%	20–25%/65–75%	10–15%/65–75%	5–10%/65–75%	(Recovery)
S80	D8RAC6_SELML	Carbonic anhydrase	*Selaginella moellendorffii*	23.6/9.83	17.3/5.94	102	49.52	7	4.85	4.32	5.23	5.46	4.48
S95	A0A078J6Z0_BRANA	Phospholipase D	*Brassica napus*	92.4/5.93	16.7/5.10	64	32.14	13	1.15	1.05	−1.64	−1.52	1.11
	Antioxidation												
S19	B3TLY5_ELAGV	Catalase	*Elaeis guineensis* var. *tenera*	57.3/6.47	55.5/6.65	125	28.25	10	2.69	1.57	−1.01	−1.14	−5.84
S32	B8XF12_ONCHC	Monodehydroascorbate reductase	*Oncidium* hybrid cultivar	46.8/5.26	44.2/5.62	314	58.85	15	−1.40	−1.01	−2.04	−1.57	−2.32
S41	P2_ARATH	NADP-dependent alkenal double bond reductase P2	*Arabidopsis thaliana*	38.2/8.09	34.1/6.24	175	41.11	6	1.80	1.48	−1.16	1.07	1.37
S53	M4H7E2_ONCHC	Chloroplast L-ascorbate peroxidase isoform 1	*Oncidium* hybrid cultivar	41.4/8.74	28.7/5.89	356	70.90	15	1.29	1.11	1.16	1.41	1.67
S71	Q42661_CAPAN	L-ascorbate peroxidase	*Capsicum annuum*	27.7/5.32	20.4/6.23	270	66.00	7	−1.38	−1.23	−1.63	−1.53	−1.46
S87	B3TM10_ELAGV	Cytosolic ascorbate peroxidase	*Elaeis guineensis* var. *tenera*	27.5/5.42	20.5/5.48	330	69.88	6	−1.09	−1.02	−1.48	−1.29	−1.84
S89	B8XF08_ONCHC	Ascorbate peroxidase	*Oncidium* hybrid cultivar	27.6/5.31	20.7/5.38	435	71.49	6	−1.15	1.00	−3.50	−1.73	−1.37
S96	D5FUD7_VIGRA	2-Cys peroxiredoxin	*Vigna radiata*	28.7/5.50	16.1/5.07	182	46.74	7	1.04	1.11	−1.59	−1.22	1.10
S100	R4USJ3_9APIA	Glutathione peroxidase	*Eleutherococcus senticosus*	18.9/8.30	14.4/5.97	181	57.99	7	−1.59	−2.35	−2.14	−1.15	1.50
S102	A0A0B2QBV7_GLYSO	Peroxiredoxin-2E−1, chloroplastic	*Glycine soja*	18.8/7.71	11.0/5.51	143	44.83	3	1.06	−1.03	−1.94	1.08	1.03
	Proteinkinase and phosphatase												
S27	J3M8H8_ORYBR	Phosphoglycerate kinase	*Oryza brachyantha*	42.9/5.30	42.6/6.08	285	41.42	10	2.37	1.42	1.23	1.64	1.58
S38	Q9SPH7_BETVU	Phosphoribulokinase	*Beta vulgaris* subsp. *vulgaris*	30.8/5.15	38.1/5.44	320	77.12	9	−1.04	−1.16	−2.56	−1.56	−1.15
S39	KPPR_SPIOL	Phosphoribulokinase, chloroplastic	*Spinacia oleracea*	45.3/5.82	38.3/5.36	381	55.47	9	−1.12	1.15	−2.19	−1.51	−1.05

Table 1 (continued)

Spot no.	Uniprot accession no.	Protein name	Species	Exp.Mw/pI	Theo. Mw/pI	Score	Coverage	Matched peptide	Radio				
									40–45%/65–75%	20–25%/65–75%	10–15%/65–75%	5–10%/65–75%	(Recovery)
S56	Y5707_ARATH	Probable receptor-like protein kinase At5g47070	*Arabidopsis thaliana*	47.0/9.57	30.0/5.61	71	57.56	15	1.14	2.10	1.02	1.93	1.43
S62	B9RM24_RICCO	4-Nitrophenylphosphatase, putative	*Ricinus communis*	40.0/8.76	28.5/5.51	169	54.72	10	1.47	2.97	1.10	1.47	1.29
	Protein synthesis, degradation and refolding												
S4	M8C5V4_AEGTA	Aromatic-L-amino-acid decarboxylase	*Aegilops tauschii*	55.3/5.24	72.9/5.86	85	43.63	18	1.10	1.02	−1.52	1.03	1.09
S11	A0A0B2NVB9_GLYSO	Chaperonin CPN60-2, mitochondrial	*Glycine soja*	61.5/5.75	61.6/5.64	230	53.57	14	1.03	−1.23	−1.56	−1.65	1.03
S15	D7MLS6_ARALL	ATP binding protein	*Arabidopsis lyrata* subsp. *lyrata*	63.7/5.73	61.0/5.48	460	60.13	16	1.18	1.04	−1.73	−1.52	1.13
S16	W9QWD3_9ROSA	RuBisCO large subunit-binding protein subunit beta	*Morus notabilis*	83.6/5.58	61.5/5.44	416	44.73	17	1.02	1.08	−1.55	−1.49	−1.18
S17	A0A0B0MWF4_GOSAR	Heat shock 70 kDa 6, chloroplastic-like protein	*Gossypium arboreum*	74.7/5.25	72.5/4.99	628	62.79	23	−1.11	−1.02	−2.00	1.07	1.07
S18	RUBA_WHEAT	RuBisCO large subunit-binding protein subunit alpha, chloroplastic	*Triticum aestivum*	57.7/4.83	58.9/5.17	193	53.04	10	1.03	1.26	−2.34	−1.74	1.23
S24	A0A0B0NR86_GOSAR	Aspartate aminotransferase	*Gossypium arboreum*	51.1/7.12	41.8/6.53	226	40.73	10	1.79	2.43	1.60	3.99	4.88
S34	I1GKA8_BRADI	Delta-aminolevulinic acid dehydratase	*Brachypodium distachyon*	46.7/5.63	44.0/5.47	334	51.29	11	−1.65	−1.37	−3.73	−4.05	−1.85
S52	A0A078HFS6_BRANA	BnaCnng08040D protein	*Brassica napus*	34.5/5.83	28.2/6.46	117	33.33	7	7.63	3.99	2.73	3.95	2.92
S66	Q0WMZ3_ARATH	Seed maturation protein	*Arabidopsis thaliana*	67.2/5.78	25.4/5.86	78	43.46	23	1.15	6.76	1.83	13.33	2.09
S72	W9SCH1_9ROSA	Protein GRIP	*Morus notabilis*	14.1/5.25	18.2/6.57	66	25.44	26	2.00	1.84	1.03	1.43	1.44
S73	I6WTS2_9POAL	Cysteine proteinase inhibitor	*Secale cereale* × *Triticum aestivum*	26.6/6.37	17.7/6.52	101	44.03	7	2.14	1.82	1.15	1.59	−1.08

Table 1 (continued)

Spot no.	Uniprot accession no.	Protein name	Species	Exp.Mw/pI	Theo. Mw/pI	Score	Coverage	Matched peptide	Radio				
									40–45%/65–75%	20–25%/65–75%	10–15%/65–75%	5–10%/65–75%	(Recovery)
	Transcriptional and signal factor												
S30	I1JXC1_SOYBN	Elongation factor Tu	*Glycine max*	52.3/6.21	43.2/5.76	266	52.29	13	1.14	−1.21	−2.44	−1.27	1.05
S31	EFTU1_SOYBN	Elongation factor Tu, chloroplastic	*Glycine max*	52.2/6.21	43.1/5.68	267	49.06	12	1.16	1.10	−3.46	−1.74	−2.19
S40	A0A078E0H4_BRANA	Eukaryotic translation initiation factor 3 subunit A	*Brassica napus*	99.1/8.59	42.1/5.06	74	36.21	24	−1.22	−1.12	−2.00	−1.30	−1.20
S43	D3WBK9_9AQUA	DNA-directed RNA polymerase subunit beta″	*Ilex cornuta*	15.7/9.3	35.8/5.75	99	26.37	31	1.03	−1.09	−1.67	−2.61	−1.29
S54	U5FWD6_POPTR	Cysteine synthase	*Populus trichocarpa*	42.9/9.05	30.8/5.80	222	56.97	10	1.05	2.17	−1.02	−1.30	1.03
S69	A0A061ER16_THECC	NAD(P)-binding Rossmann-fold superfamily protein isoform 1	*Theobroma cacao*	36.5/9.29	21.5/6.27	338	52.55	7	1.05	1.03	1.06	1.43	−1.22
S74	B9HK78_POPTR	Uridylyltransferase-related family protein	*Populus trichocarpa*	22.2/6.30	24.9/5.04	198	66.50	7	1.53	−1.04	−1.21	−1.35	−1.04
S85	A0A078GD20_BRANA	BnaCnng04720D protein	*Brassica napus*	46.1/8.14	21.5/5.55	69	49.25	16	1.01	1.22	1.69	1.18	1.31
S86	B3TLW0_ELAGV	Glutathione *S*-transferase	*Elaeis guineensis* var. *tenera*	27.6/5.53	21.7/5.46	96	39.00	6	−1.89	1.26	−2.11	1.18	1.01
S88	W9QRR6_9ROSA	Ribosomal protein S10	Morus notabilis	31.6/11.2	21.9/5.37	71	62.55	14	3.73	1.00	2.25	1.28	−1.66
S90	G7KFH4_MEDTR	Brefeldin A-inhibited guanine nucleotide-exchange protein	*Medicago truncatula*	19.0/5.70	18.7/5.49	73	23.22	30	−1.46	−1.54	−1.48	−1.27	1.17
	Cell structure and division												
S5	K7KSM4_SOYBN	Kinesin-like protein	*Glycine max*	82.4/6.00	71.7/5.49	79	47.40	20	−1.58	−1.07	−2.43	−2.01	−1.92
S59	D8U105_VOLCA	Flagellar inner arm dynein 1 heavy chain beta	*Volvox carteri* f. *nagariensis*	51.4/6.02	30.3/5.41	86	12.82	53	−1.30	2.96	−1.09	3.42	1.65
S65	G7JMW8_MEDTR	Myosin II heavy chain family protein	*Medicago truncatula*	65.3/9.11	25.4/5.96	82	49.38	27	−3.83	−1.97	−3.18	−2.53	−1.05
S82	D7LUM1_ARALL	Tubulin family protein	*Arabidopsis lyrata* subsp. *lyrata*	86.2/6.37	17.8/5.71	89	32.62	24	1.43	1.50	−1.07	−1.10	1.45
S103	A0A0B2Q6P6_GLYSO	Kinesin-like protein	*Glycine soja*	61.0/9.77	14.1/5.19	67	33.82	20	−1.94	−1.95	−3.83	−4.59	−3.85

Table 1 (continued)

Spot no.	Uniprot accession no.	Protein name	Species	Exp.Mw/pI	Theo. Mw/pI	Score	Coverage	Matched peptide	Radio				
									40–45%/65–75%	20–25%/65–75%	10–15%/65–75%	5–10%/65–75%	(Recovery)
C. tracyanum													
	Photosynthesis												
T5	N1QRT3_AEGTA	Endoplasmin	*Aegilops tauschii*	139/5.49	93.8/4.87	331	28.91	19	−1.32	−1.20	1.12	−1.50	1.32
T8	FTSH1_ARATH	ATP-dependent zinc metalloprotease FTSH 1, chloroplastic	*Arabidopsis thaliana*	76.9/5.64	77.6/5.64	110	43.16	18	1.48	−1.21	−1.28	−1.19	1.25
T17	B9IA25_POPTR	FtsH-like protein Pftf	*Populus trichocarpa*	74.4/6.06	74.4/5.51	474	48.92	15	−1.23	1.39	−1.41	−2.21	−1.26
T22	W8SJN1_9POAL	6-Phosphogluconate dehydrogenase, decarboxylating	*Saccharum* hybrid cultivar Yacheng05-179	52.8/5.93	55.7/6.00	107	46.67	12	1.32	1.33	1.36	1.03	−1.49
T44	Q20ET7_OLTVI	Mg-protoporphyrin IX chelatase	*Oltmannsiellopsis viridis*	39.7/4.70	43.2/5.54	125	57.42	12	−4.26	1.33	−2.07	−2.36	−3.09
T55	FENR_VICFA	Ferredoxin--NADP reductase, chloroplastic	*Vicia faba*	40.8/8.7	34.6/6.54	272	113.77	12	1.72	1.13	2.03	2.06	2.05
T66	G7ZYV5_MEDTR	Oxygen-evolving enhancer protein	*Medicago truncatula*	27.4/8.29	27.3/5.49	158	43.14	7	1.43	1.25	1.52	−1.17	1.12
T67	A6N1L3_ORYSI	Oxygen-evolving enhancer protein 1	*Oryza sativa* subsp. *indica*	19.0/4.79	25.9/5.42	91	33.71	2	1.84	1.62	1.10	−1.04	1.44
T69	A0A0B2RSW1_GLYSO	Oxygen-evolving enhancer protein 1, chloroplastic	*Glycine soja*	35.0/6.48	27.0/5.36	270	65.05	12	1.76	1.29	1.52	1.18	1.10
T71	I0B7J2_NICBE	Chloroplast PsbO2	*Nicotiana benthamiana*	35.4/5.61	27.6/5.23	239	53.01	10	1.60	1.38	1.57	−1.19	1.03
T76	A0A061ER16_THECC	NAD(P)-binding Rossmann-fold superfamily protein isoform 1	*Theobroma cacao*	36.5/9.29	24.4/6.65	300	42.34	8	1.46	1.87	2.29	3.00	2.66
T86	A0A0B2R7F2_GLYSO	Chlorophyll *a–b* binding protein CP26, chloroplastic	*Glycine soja*	31.0/5.72	20.6/5.60	307	40.55	6	1.57	1.14	1.38	1.30	1.79
T88	A0A0B0MHC6_GOSAR	Chlorophyll *a–b* binding 6A, chloroplastic	*Gossypium arboreum*	27.0/6.22	17.5/6.00	170	38.87	5	1.41	1.06	1.47	2.41	−1.33
T90	I0B7J7_NICBE	Chloroplast PsbP3	*Nicotiana benthamiana*	28.7/6.84	19.1/5.25	97	19.40	2	3.32	1.41	1.65	1.03	1.35

Table 1 (continued)

Spot no.	Uniprot accession no.	Protein name	Species	Exp.Mw/pI	Theo. Mw/pI	Score	Coverage	Matched peptide	Radio				
									40–45%/65–75%	20–25%/65–75%	10–15%/65–75%	5–10%/65–75%	(Recovery)
T92	V9LU30_DENLA	Light harvesting chlorophyll *a*/*b*-binding protein 2-1	*Dendrocalamus latiflorus*	28.6/5.62	19.6/5.03	132	19.01	3	2.01	1.22	1.04	1.10	5.59
T95	A0A072VAK2_MEDTR	Light-harvesting complex I chlorophyll A/B-binding protein	*Medicago truncatula*	25.9/4.96	20.1/4.78	135	22.78	4	1.72	−1.00	1.93	−1.08	1.19
T100	F6HTI7_VITVI	Cytochrome b6-f complex iron-sulfur subunit	*Vitis vinifera*	20.9/6.88	13.3/6.24	180	40.72	4	2.30	1.40	2.16	1.36	1.53
	Defense response												
T14	F2D550_HORVD	Malic enzyme	*Hordeum vulgare* var. *distichum*	75.7/7.73	79.0/6.59	111	12.99	7	1.33	1.37	−1.02	1.41	1.53
T15	D2E9R6_DACGL	Hsp organizing protein/stress-inducible protein	*Dactylis glomerata*	64.8/6.11	79.7/6.55	165	33.39	11	2.75	2.45	1.58	2.05	2.03
T34	A0A0A0LII5_CUCSA	Malate dehydrogenase	*Cucumis sativus*	36.1/5.76	40.9/6.46	194	27.03	5	1.59	1.36	1.13	−1.08	1.07
T56	D3YJ40_9LAMI	Phenylcoumaran benzylic ether reductase-like protein	*Salvia fruticosa*	33.8/6.01	32.1/6.58	125	13.07	2	1.87	1.03	1.90	2.19	1.60
T79	SARED_ESCCA	Sanguinarine reductase	*Eschscholzia californica*	29.6/4.97	23.7/6.20	255	24.18	2	1.55	−1.04	1.51	1.26	1.22
T83	K7M833_SOYBN	Ferritin	*Glycine max*	29.9/5.56	21.3/5.87	143	49.06	5	1.35	1.62	3.19	2.02	4.07
	Carbon and energy metabolism												
T1	F6LR34_9ASPA	Phosphoenolpyruvate carboxylase	*Dendrobium catenatum*	110.0/6.00	105.8/6.54	89	28.53	25	2.20	1.60	1.55	1.11	1.13
T2	O23928_9POAL	Pyruvate orthophosphate dikinase	*Eleocharis vivipara*	96.7/5.21	98.6/5.86	234	34.62	15	−1.77	−1.30	−1.09	−1.29	−2.04
T6	W9RGS5_9ROSA	Transketolase	*Morus notabilis*	80.7/6.31	82.7/5.94	94	22.52	14	−1.15	−1.53	−1.44	−1.26	−1.16
T7	A9SLW6_PHYPA	Inner dynein arm 1 heavy chain 1-ALPHa	*Physcomitrella patens* subsp. *patens*	52.2/5.6	82.9/5.89	102	12.79	63	−1.07	−1.26	1.69	1.08	1.21
T10	G7KXT9_MEDTR	Heat shock cognate 70 kDa protein	*Medicago truncatula*	71.4/5.08	79.9/5.33	194	35.44	12	1.19	1.16	1.02	−2.65	−1.62
T11	HSP70_MAIZE	Heat shock 70 kDa protein	*Zea mays*	70.9/5.22	80.7/5.29	213	32.25	14	−1.80	−1.32	1.32	−1.18	1.55
T12	C9WCK6_9MARC	Heat shock protein 70	*Pellia endiviifolia*	71.5/5.03	83.1/5.25	215	57.60	22	1.16	1.52	1.66	−1.32	2.80

Table 1 (continued)

Spot no.	Uniprot accession no.	Protein name	Species	Exp.Mw/pI	Theo. Mw/pI	Score	Coverage	Matched peptide	Radio				
									40–45%/65–75%	20–25%/65–75%	10–15%/65–75%	5–10%/65–75%	(Recovery)
T16	W9RHR9_9ROSA	ATP-dependent zinc metalloprotease FTSH 2	*Morus notabilis*	74.4/5.94	73.2/5.56	936	68.59	20	1.54	1.05	1.34	1.40	1.16
T24	R4QG39_9ASPA	ATP synthase subunit beta	*Cymbidium goeringii*	52/5.34	58.8/5.73	450	88.77	17	1.29	−1.10	1.45	1.43	1.31
T25	M9YXY4_9ASPA	ATP synthase subunit beta, chloroplastic	*Cymbidium aloifolium*	53.9/5.37	59.9/5.64	738	120.68	25	1.58	−1.03	2.40	2.61	1.81
T26	M9YRN0_9ASPA	ATP synthase subunit alpha, chloroplastic	*Cymbidium tracyanum*	55.3/5.27	62.3/5.60	698	67.65	19	1.55	−1.53	1.16	1.52	1.31
T27	Q6Y643_BAMOL	UDP-glucose pyrophosphorylase	*Bambusa oldhamii*	52.1/5.35	60.5/5.51	209	30.02	7	−1.21	−1.59	−1.17	1.15	1.47
T28	UGPA_HORVU	UTP--glucose-1-phosphate uridylyltransferase	*Hordeum vulgare*	51.8/5.20	60.4/5.36	205	29.60	8	1.29	1.10	−1.88	−1.23	−1.26
T29	G7KNB8_MEDTR	Phosphopyruvate hydratase	*Medicago truncatula*	46.5/5.9	58.6/5.28	259	70.40	13	1.53	1.44	−1.08	1.31	1.04
T30	ENO_POPEU	Enolase	*Populus euphratica*	2.75/4.79	58.3/5.23	82	200.00	2	1.15	−1.71	1.69	−1.02	1.22
T31	K8E991_9CHLO	Glyceraldehyde-3-phosphate dehydrogenase	*Bathycoccus prasinos*	43.4/6.46	49.9/6.61	234	29.38	7	2.37	1.62	1.21	1.50	1.84
T33	W1PF21_AMBTC	Fructose-bisphosphate aldolase	*Amborella trichopoda*	42.7/8.14	41.6/6.51	121	29.26	8	1.74	1.03	2.33	2.12	2.49
T36	I1QF99_ORYGL	Glyceraldehyde-3-phosphate dehydrogenase	*Oryza glaberrima*	37.6/6.11	42.6/6.31	356	41.09	7	3.39	2.14	3.01	1.90	2.44
T40	Q8GTY4_MEDSA	Rubisco activase	*Medicago sativa*	30.2/5.63	44.9/5.82	395	76.67	9	1.81	1.57	1.58	1.18	1.29
T41	K7RYG4_GOSBA	Chloroplast ribulose bisphosphate carboxylase/oxygenase activase beta2	*Gossypium barbadense*	33.1/5.09	45.3/5.66	281	75.34	13	1.82	1.23	1.74	1.32	1.21
T42	W9S2F0_9ROSA	Ribulose bisphosphate carboxylase/oxygenase activase 1	*Morus notabilis*	52.1/6.39	51.5/5.54	482	46.95	11	1.59	1.41	1.50	1.12	1.58

Table 1 (continued)

Spot no.	Uniprot accession no.	Protein name	Species	Exp.Mw/pI	Theo. Mw/pI	Score	Coverage	Matched peptide	Radio				
									40–45%/65–75%	20–25%/65–75%	10–15%/65–75%	5–10%/65–75%	(Recovery)
T46	A0A0A0YQW8_GARJA	Putative Rubisco activase isoform 2	*Gardenia jasminoides*	52.3/5.26	52.0/5.42	485	47.79	12	1.38	1.33	1.50	1.07	1.16
T48	C3URF6_PHYFE	Phosphoribulokinase	*Physaria fendleri*	25.9/5.01	42.5/5.42	211	51.11	6	1.71	−1.04	1.27	1.36	1.36
T49	V5NC92_9ROSA	Ribulose bisphosphate carboxylase/oxygenase activase 2	*Pyrus x bretschneideri*	53.2/5.97	52.6/5.32	345	43.66	10	2.11	1.95	1.96	1.54	1.52
T57	B9A9C9_MORAL	Urease accessory protein ureG	*Morus alba*	30.6/5.93	32.6/6.10	311	84.59	10	1.46	1.44	1.63	1.26	1.30
T63	M8CSF4_AEGTA	Disease resistance protein RPP13	*Aegilops tauschii*	16.5/8.81	33.5/5.57	62	28.84	26	1.02	1.03	1.57	1.03	−1.38
T74	A0A061DFL1_THECC	Gamma carbonic anhydrase 1, CA1	*Theobroma cacao*	29.7/6.32	27.0/6.37	175	65.68	8	1.09	1.40	1.04	1.47	−1.21
T80	V4LAM9_EUTSA	Ribulose-phosphate 3-epimerase	*Eutrema salsugineum*	29.6/8.30	21.7/6.44	190	49.09	6	2.63	1.06	2.40	3.33	2.12
T84	TPIC_SECCE	Triosephosphate isomerase, chloroplastic	*Secale cereale*	32.0/6.00	22.2/5.82	167	44.63	9	1.61	1.30	1.25	1.16	1.23
T81	D8R755_SELML	Carbonic anhydrase	*Selaginella moellendorffii*	25.8/8.79	20.7/6.17	78	26.64	4	1.80	1.24	1.59	1.55	1.71
T98	A0A061FUR0_THECC	ATP synthase D chain, mitochondrial	*Theobroma cacao*	19.7/5.21	15.7/5.06	117	38.10	3	1.70	−1.17	1.20	−1.01	−1.05
T99	A0A061F8S8_THECC	ATP synthase delta-subunit protein	*Theobroma cacao*	25.9/7.88	16.1/4.92	216	38.75	5	1.66	−1.04	1.58	2.54	1.15
	Antioxidation												
T37	U3PV73_ARTAN	Double bond reductase	*Artemisia annua*	38.3/6.04	38.8/6.22	116	33.91	6	1.27	−1.01	1.52	1.47	−1.26
T43	B3TLY7_ELAGV	Disulfide-isomerase-like protein	*Elaeis guineensis* var. *tenera*	40.6/5.37	41.9/5.61	215	38.57	8	1.39	1.60	1.32	1.26	1.21
T54	A0A0A1CE86_9MAGN	NADPH:quinone reductase	*Paeonia cathayana*	12.8/5.81	34.5/5.31	193	18.85	1	1.29	−1.74	1.13	2.28	1.18
T59	W9S8N9_9ROSA	Quinone oxidoreductase-like protein	*Morus notabilis*	33.8/8.37	36.6/5.84	116	27.90	6	1.02	−1.52	1.16	1.49	−2.11

Table 1 (continued)

Spot no.	Uniprot accession no.	Protein name	Species	Exp.Mw/pI	Theo. Mw/pI	Score	Coverage	Matched peptide	Radio				
									40–45%/65–75%	20–25%/65–75%	10–15%/65–75%	5–10%/65–75%	(Recovery)
T73	CDSP_ARATH	Thioredoxin-like protein CDSP32, chloroplastic	*Arabidopsis thaliana*	33.9/8.65	28.1/6.52	129	38.74	8	1.76	1.06	1.97	1.58	1.20
T75	A0A078C8P7_BRANA	BnaC06g36750D protein	*Brassica napus*	34.4/8.40	28.0/6.36	115	24.18	5	1.15	1.15	1.70	1.34	1.22
T77	B8XF08_ONCHC	Ascorbate peroxidase	*Oncidium hybrid cultivar*	27.6/5.31	23.7/6.35	83	25.70	3	1.06	1.77	−1.40	1.17	1.09
T85	B8XF08_ONCHC	Ascorbate peroxidase	*Oncidium hybrid cultivar*	27.6/5.31	22.4/5.64	168	40.56	4	1.61	1.22	1.37	1.18	1.15
T93	Q012L2_OSTTA	Thioredoxin-like fold	*Ostreococcus tauri*	26.0/5.21	18.5/5.00	89	9.57	1	1.95	−1.07	1.35	1.17	1.46
T94	I0CC94_9CARY	2-cys peroxiredoxin	*Tamarix hispida*	30.0/6.90	17.4/5.12	122	29.20	4	2.12	1.01	1.82	1.28	1.81
T96	R4USJ3_9APIA	Glutathione peroxidase	*Eleutherococcus senticosus*	18.9/8.30	15.7/5.62	161	66.86	7	1.45	1.14	1.12	1.03	1.20
T97	B8YNY0_GINBI	Superoxide dismutase	*Ginkgo biloba*	21.9/6.75	14.9/5.35	381	71.36	7	1.39	2.32	1.42	1.44	1.38
T101	D8SBS8_SELML	Superoxide dismutase	*Selaginella moellendorffii*	15.5/5.59	11.1/5.66	101	30.46	2	1.33	1.83	1.79	1.24	1.01
T102	A0A0B2P3S7_GLYSO	Peroxiredoxin-2E, chloroplastic	*Glycine soja*	19.7/5.08	12.0/5.22	79	32.61	3	1.94	−1.13	1.33	1.38	1.76
T103	A0A077D9N5_TOBAC	Thioredoxin peroxidase 1	*Nicotiana tabacum*	17.5/5.34	10.3/5.29	84	29.01	3	1.64	1.05	1.29	1.39	1.33
T104	I3SQE3_MEDTR	Type II peroxiredoxin	*Medicago truncatula*	23.3/8.45	10.4/5.22	77	24.42	2	1.99	−1.02	1.57	2.02	1.76
	Proteinkinase and phosphatase												
T38	A5CAF6_VITVI	Phosphoglycerate kinase	*Vitis vinifera*	42.5/6.29	47.2/6.02	309	47.38	11	1.73	2.18	2.18	1.58	1.45
T50	KPPR_SPIOL	Phosphoribulokinase, chloroplastic	*Spinacia oleracea*	45.3/5.82	43.1/5.33	355	50.75	7	3.31	2.42	2.84	2.46	2.31
T53	E5GC94_CUCME	Fructokinase	*Cucumis melo* subsp. *melo*	35.8/5.61	37.4/5.18	222	27.79	6	2.38	−1.37	1.21	1.75	1.81
T70	M8C200_AEGTA	Phosphoglycolate phosphatase	*Aegilops tauschii*	33.7/4.93	20.3/4.79	305	39.22	6	1.40	1.67	1.10	−1.01	−1.10

Table 1 (continued)

Spot no.	Uniprot accession no.	Protein name	Species	Exp.Mw/pI	Theo. Mw/pI	Score	Coverage	Matched peptide	Radio				
									40–45%/65–75%	20–25%/65–75%	10–15%/65–75%	5–10%/65–75%	(Recovery)
	Protein synthesis, degradation and refolding												
T4	A0A061FKM2_THECC	Chaperone protein htpG family protein isoform 2	*Theobroma cacao*	93.8/4.88	99.2/5.04	208	22.21	16	1.11	−1.57	−1.18	−2.68	−1.24
T9	A0A0A7LWK6_9ASPA	Heat shock 70 kDa protein	*Albuca bracteata*	73.1/5.73	76.2/5.57	160	27.98	10	1.06	1.11	−1.14	−1.52	−1.31
T13	E5FQ64_PENAM	Heat shock protein 90	*Pennisetum americanum*	80.6/5.00	89.2/5.15	428	59.03	21	1.38	1.39	1.35	−1.82	1.46
T18	CPNB2_ARATH	Chaperonin 60 subunit beta 2, chloroplastic	*Arabidopsis thaliana*	63.7/5.60	68.3/5.38	325	35.07	11	1.65	1.44	1.01	1.21	1.44
T19	A0A078H2L0_BRANA	BnaC09g33020D protein	*Brassica napus*	63.3/5.86	70.0/5.33	386	57.58	17	3.43	1.83	1.99	2.58	2.78
T20	Q7X9A7_ORYSJ	60 kDa chaperonin alpha subunit	*Oryza sativa* subsp. *japonica*	61.5/5.36	68.9/5.11	182	43.66	10	1.39	−1.14	1.10	1.08	1.41
T32	B9IL28_POPTR	Aspartate aminotransferase	*Populus trichocarpa*	51.1/8.67	48.4/6.48	245	42.06	11	2.45	1.67	2.19	2.11	2.06
T35	B9R7X3_RICCO	Ornithine carbamoyltransferase, putative	*Ricinus communis*	41.7/7.20	38.8/6.41	171	24.60	5	1.35	−1.55	−1.14	−1.91	1.21
T47	I1GKA8_BRADI	Delta-aminolevulinic acid dehydratase	*Brachypodium distachyon*	46.7/5.63	49.7/5.42	309	50.82	12	1.19	1.64	1.36	1.14	1.27
T60	M0SZ91_MUSAM	Cysteine synthase	*Musa acuminata* subsp. *malaccensis*	41.4/6.78	28.2/5.97	105	25.00	4	−5.63	1.10	5.43	1.73	−5.12
T89	A0A022QH46_ERYGU	Proteasome subunit beta type	*Erythranthe guttata*	25.2/5.03	18.8/5.77	169	47.03	7	1.42	−1.01	1.42	2.52	−1.22
T91	A0A061RXL1_9CHLO	Mitochondrial inner membrane protease subunit 1	*Tetraselmis* sp. GSL018	20.4/8.83	17.3/5.27	65	71.02	10	1.63	−1.06	1.01	1.13	1.39
	Transcriptional and signal factor												
T21	G8HAA9_PAPSO	PLP-dependent aminotransferase	*Papaver somniferum*	53.6/6.16	58.9/6.45	281	51.04	8	2.00	−1.17	1.33	1.57	1.52
T23	G7LGN1_MEDTR	Drug resistance transporter-like ABC domain protein	*Medicago truncatula*	148.0/6.96	58.1/5.95	78	27.98	30	1.14	1.41	1.31	1.05	−1.32
T39	G7JFU3_MEDTR	Arginase family protein	*Medicago truncatula*	26.3/5.99	40.5/5.99	146	47.28	6	2.02	1.39	2.17	1.47	2.10

Table 1 (continued)

Spot no.	Uniprot accession no.	Protein name	Species	Exp.Mw/pI	Theo. Mw/pI	Score	Coverage	Matched peptide	Radio				
									40–45%/65–75%	20–25%/65–75%	10–15%/65–75%	5–10%/65–75%	(Recovery)
T45	B6T782_MAIZE	40S ribosomal protein SA	*Zea mays*	33.6/4.94	41.8/5.49	190	45.45	8	1.45	−1.06	1.16	−1.15	1.25
T51	B9RCP6_RICCO	Grave disease carrier protein, putative	*Ricinus communis*	38.7/9.51	38.8/5.41	71	47.61	15	−1.05	−2.15	1.06	1.41	1.66
T52	A0A088CKL2_9CHLO	DNA-directed RNA polymerase subunit	*Prasinophyceae* sp. MBIC10622	21.8/9.88	37.5/5.34	69	22.19	31	3.84	1.67	2.24	3.24	2.24
T61	W9SQD6_9ROSA	Bifunctional dihydroflavonol 4-reductase/flavanone 4-reductase	*Morus notabilis*	25.6/5.77	31.6/5.84	87	27.07	4	2.63	1.36	1.92	1.78	1.06
T64	M0U0S6_MUSAM	Lactoylglutathione lyase	*Musa acuminata* subsp. *malaccensis*	29.5/5.35	29.5/5.68	205	82.06	15	1.26	1.60	1.10	−1.02	1.16
T65	A0A078E4S0_BRANA	BnaA07g26290D protein	*Brassica napus*	38.2/6.49	29.2/5.53	127	53.37	13	1.43	1.49	1.65	1.11	1.23
T68	A0A0B2NZ09_GLYSO	Glutathione S-transferase L3	*Glycine soja*	28.2/5.35	25.4/5.34	94	31.05	4	1.69	1.42	1.72	1.19	−1.10
T72	B9HK78_POPTR	Uridylyltransferase-related family protein	*Populus trichocarpa*	22.2/6.30	28.4/5.04	178	48.28	6	1.56	1.24	1.54	−1.02	1.19
T78	W6JJB4_NICBE	Nuclear pore complex protein TPRb	*Nicotiana benthamiana*	23.0/4.89	26.3/6.15	79	26.80	41	1.83	1.72	1.37	2.19	1.32
T82	G7I4U4_MEDTR	Plastid fibrillin	*Medicago truncatula*	29.8/6.91	23.4/5.92	85	31.16	7	1.76	1.41	1.44	−1.00	1.41
T87	G7J3X9_MEDTR	General regulatory factor 2	*Medicago truncatula*	29.4/4.71	22.3/5.00	108	73.85	12	1.54	1.13	−1.01	−1.24	1.17
	Cell structure and division												
T58	A0A078DV04_BRANA	BnaA05g21080D protein	*Brassica napus*	31.3/5.11	33.0/6.04	82	23.35	49	1.92	1.43	1.67	1.46	1.44
T62	D9CJ76_VOLCA	DHC1bm	*Volvox carteri f. nagariensis*	48.7/6.18	33.5/5.78	91	17.45	56	1.04	1.22	1.06	−2.52	1.58
T3	W9RWY6_9ROSA	Cell division cycle protein 48-like protein	*Morus notabilis*	88.5/5.05	99.0/5.44	829	67.26	33	−1.13	−1.14	1.31	−1.65	−1.67

RWC dropped to 10–45%, possibly contributing to the rise in the JA concentration.

Photoprotection of *C. sinense* and *C. tracyanum*

During the drought-treatment period, the leaf water status in *C. sinense* and *C. tracyanum* was stabilized because of the rapid closure of stomata. However, such quick activity can limit CO_2 uptake and the utilization of absorbed light energy. Redundant energy will lead to an over-accumulation of electrons in photosynthetic electron transfer chain, which can then result in photoinhibition. However, we detected no significant change in the values for F_v/F_m in dark-adapted leaves and in P_m for either species under drought stress, thereby indicating that the activities of PSII and PSI were not influenced by photoinhibition. While some proteins were found to be involved in linear electron flow (LEF) from water to $NADP^+$ via PSII and PSI in series and cyclic electron flow (CEF) around PSI, our proteomics analysis showed that these proteins had either a positive or negative response to drought stress. When we compared the changes in proteins between species, we found that *C. tracyanum* had greater capacity for photoprotection, resulting in little risk of photoinhibition for PSII, effectively balance between CEF and LEF and increasing photorespiration.

Within the photosynthetic machinery, PSII is particularly sensitive to abiotic stresses, and its photoinhibition is determined by the balance between the rate of photodamage and repair (Nishiyama et al. 2006). Both oxygen-evolving enhancer protein and two other molecules (33 and 17 kDa) form an oxygen-evolving complex (James et al. 1989) that is associated with PSII photodamage (Ohnishi et al. 2005). For *C. sinense*, the expression level of oxygen-evolving enhancer protein (Table 1; spot S68, spot S94) was down-regulated when soil RWC dropped down to either 40–45 or 10–15%. This also occurred during the recovery. However, the expression of oxygen-evolving enhancer protein (Table 1; spot T66, spot T67, spot T69) in *C. tracyanum* was up-regulated at soil RWC of 40–45, 20–25 and 10–15%. Repairing PSII photodamage requires several steps: degradation of damaged D1 protein; de novo synthesis of D1 protein; and installation of the newly synthesized D1 protein into PSII (Takahashi and Murata 2008). In the chloroplasts of *Arabidopsis*, FtsH2 and FtsH5 participate in the repair of photodamaged PSII by digesting and removing damaged D1 protein (Bailey et al. 2002; Sakamoto et al. 2002). The FtsH proteases are involved in the primary cleavage of the D1 protein under moderate heat stress (Yoshioka et al. 2006). We found that, in *C. tracyanum*, the FtsH-like protein Pftf (Table 1; spot T17) was down-regulated as soil RWC decreased to 5–10%, but was recovered as the stress abated. This indicated that there was little risk of PSII photoinhibition in *C. tracyanum* under more severe drought conditions.

Cyclic electron flow is an important mechanism for protecting PSI and PSII against the effects of drought stress (Lehtimäki et al. 2010; Huang et al. 2013). Here, CEF was more strongly stimulated in *C. tracyanum* than in *C. sinense*. Furthermore, the level of ferredoxin-NADP reductase (FNRs) was up-regulated during the stress period and recover phase, but only for *C. tracyanum* (Table 1; spot T55). The physiological role of FNRs is catalyze the final step of photosynthetic electron transport, namely, the transfer of electron from the iron–sulfur protein ferredoxin (Fd) reduced by PSI to $NADP^+$ (Shin and Arnon 1965). A supercomplex mediation CEF including FNRs, has been separated in *Chlamydomonas reinhardtii*, which regulates the energy balance of PSII and PSI, and switches the mode of photosynthetic electron flow that is controlled by a photoacclimation mechanism called state transition to main cellular ATP homeostasis (Iwai et al. 2010). During the state transition from state 1 to state 2 (in which most of the excitation energy is used by PSI photochemistry, and CEF around PSI prevails over LEF) (Finazzi et al. 2002), cytochrome b_6-f complex migrates from the appressed region in the thylakoid membranes, where PSII resides, to the non-appressed region, where PSI resides (Vallon et al. 1991). Here, we determined that fluctuations in the expression of cytochrome b_6-f complex iron–sulfur subunit (Table 1; spot S99; spot T100) in both species were possibly related to the state transition, and therefore, to the balance between CEF and LEF.

Ribulose 1,5-bisphosphate carboxylase/oxygenase (Rubisco) has dual functions: CO_2 fixation and oxygenase reactions. However, because Rubisco has no binding sites for CO_2 and O_2 at the same time, so the competing reactions between the two depend upon their concentrations (Spreitzer and Salvucci 2002). Under drought stress, the reduced intercellular CO_2 concentration in a leaf that results from stomatal closure may lead to the increased oxygenation of RuBP by Rubisco and photorespiration. In *C. tracyanum*, expression of Rubisco activase was up-regulated under drought as well as recovery (Table 1; spot T41; spot T42, spot T49). Meanwhile, phosphoglycolate phosphatase (Table 1; spot T70) involved in the process of photorespiration, was also up-regulated. This demonstrated that photorespiration in *C. tracyanum* can be up-regulated by water stress. Photorespiration can help avoid inhibition of the synthesis of D1 protein, which is important for the repair of photodamaged PSII (Takahashi et al. 2007). In contrast, for *C. sinense*, some Rubisco activase (Table 1; spot S33, spot S35) was down-regulated during drought treatment, and even some proteins (Table 1; spot S29) were down-regulated when the stress relieved. These findings indicated that *C. tracyanum* can alleviate photodamage by increasing its photorespiration, thereby enhancing its adaptability to drought conditions.

Changes in the carbon balance and antioxidant activity during water stress

Sugars play a central role in plant metabolism, because they are a source of carbon and energy in cells (Pinheiro et al. 2001). However, their role in drought tolerance is debatable. For example, Ramel et al. (2009) found that the pre-stress sugar concentration is correlated with subsequent stress tolerance. In contrast, Chaves and Oliveira (2004) suggested that leaf concentrations of soluble sugars are not consistently altered in plants under drought conditions. We also did not detect any marked change in levels of soluble sugars in our stressed plants, although those concentrations were higher in *C. sinense* than in *C. tracyanum*. Starch is required as a buffer during periods of abiotic stress (Kozlowski and Pallardy 2002). In *Arabidopsis*, starch appears to be a key factor in coordinating the drought response, photosynthesis, ABA accumulations, reactive oxygen species (ROS) activation, and transcription of several amylases and sucrose synthases, and it is also possibly associated with transcription of amylase and catalase genes (Pinheiro et al. 2001). We determined that the starch concentration in *C. sinense* decreased dramatically when soil RWC dropped to 10–15%, but did not recover when the stress was alleviated. No significant changes in starch concentration were found in *C. tracyanum*. The expression of fructose-bisphosphate aldolase (Table 1; spot S42) was significantly up-regulated (7.7- to 13.1-fold) in drought-stressed plants of *C. sinense*, which possibly contributed to the decrease in starch levels there. These alterations in sugar and starch concentrations, combined with elevated levels of proteins associated with carbon metabolism, might demonstrate that the greater capacity to balance the carbon source–sink helps to improve the drought tolerance in *C. tracyanum.*

When ROS production is induced by various abiotic stresses, it can disrupt normal metabolism of plants by damaging DNA, and inhibiting the functions of proteins, chlorophyll and membranes (Alscher et al. 1997). In response to severe drought-related oxidative stress, plants trigger complex antioxidant enzymes, including SOD and CAT (Gill and Tuteja 2010). We found that the activities of both were higher in *C. sinense* than in *C. tracyanum* throughout the entire treatment period. The level of CAT in *C. sinense* (Table 1; spot S19) was up-regulated at the beginning of the drought treatment and down-regulated during recovery phase. For *C. tracyanum*, the level of SOD (Table 1; spot T97, spot T101) was continuously up-regulated through drought treatment.

The ascorbate–glutathione (ASC–GSH) cycle also has a key role in removing H_2O_2, which is catalyzed by a set of four enzymes: ascorbate peroxidase (APX), monodehydroascorbate reductase (MDHAR), glutathione-dependent dehydroascorbate reductase (DHAR), and glutathione reductase (GR). In contrast with CAT, APX, as a reductant in the first step of the ASC–GSH cycle, can efficiently remove low concentrations of H_2O_2 (Noctor and Foyer 1998). For *C. sinense*, the expression of chloroplast L-ascorbate peroxidase isoform (Table 1; spot S53) was up-regulated during water recovery. Expression level of APX of *C. tracyanum* (Table 1; spot T77, spot T85) was up-regulated during the drought period. Exogenous JA is effective in protecting plants against drought-induced oxidative damage because it can enhance the activity of antioxidant enzymes (Riemann et al. 2015). This is supported by the increase in JA levels that was found in *C. sinense*. Therefore, although the activity of antioxidant enzymes differed somewhat between two species, *C. sinense* could remedy its relatively weak capacity to prevent ROS generation under drought conditions by improving its ability to eliminate ROS.

Conclusion

We investigated the adaptive mechanisms of *C. sinense* and *C. tracyanum* to drought stress based on their morphology, physiology and proteomics. Whereas *C. sinense* appears to employ "remedy strategy", *C. tracyanum* utilizes a "precaution strategy". We have modeled these contrasting strategies for adaptations, as presented in Fig. 8. The unique water-related traits associated with their root anatomy and leaf physiology mean that *C. tracyanum* is more drought-tolerant when compared with *C. sinense*. In *C. tracyanum*, the stimulation of CEF and enhancement of photorespiration improved its photoprotection under water stress. These plants also demonstrated greater capacity to maintain carbon balance and the responded more effectively to ABA. Although the photosystem of *C. sinense* was more sensitive to drought stress, increase of phytohormones concentration

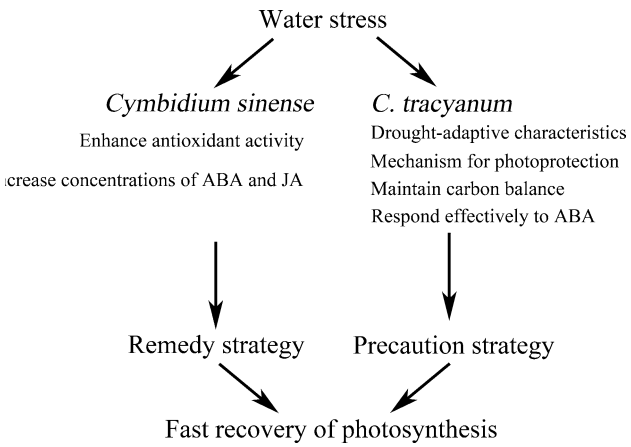

Fig. 8 Proposed model demonstrating that *Cymbidium sinense* and *C. tracyanum* employ divergent strategies in response to water stress

and antioxidant activity helped this species survive under our stress treatment. All of these findings explained the distinct water-adaptation strategies of epiphytic and terrestrial orchids, and may contribute to our understanding about the ecological adaptations of epiphytic orchids.

Author contribution statement J-WL, S-BZ and X-YH conceived and designed research; J-WL and X-DC conducted experiments; J-WL, LM and X-YH analyzed data; J-WL and S-BZ wrote the manuscript; all authors read and approved the manuscript.

Acknowledgements This work is financially supported by the National Natural Science Foundation of China (31370362, 31670342), and National Key Project of the Ministry of Science and Technology of China (2015BAD10B03).

References

Alscher RG, Donahue JL, Cramer CL (1997) Reactive oxygen species and antioxidants: relationships in green cells. Physiol Plant 100:224–233

Bailey S, Thompson E, Nixon PJ, Horton P, Mullineaux CW, Robinson C, Mann NH (2002) A critical role for the Var2 FtsH homologue of *Arabidopsis thaliana* in the photosystem II repair cycle in vivo. J Biol Chem 277:2006–2011

Benzing D, Ott D, Friedman W (1982) Roots of *Sobralia macrantha* (Orchidaceae): structure and function of the velamen-exodermis complex. Am J Bot 69:608–614

Blackman CJ, Brodribb TJ, Jordan GJ (2010) Leaf hydraulic vulnerability is related to conduit dimensions and drought resistance across a diverse range of woody angiosperms. New Phytol 188:1113–1123

Bonhomme L, Monclus R, Vincent D, Carpin S, Lomenech AM, Plomion C, Brignolas F, Morabito D (2009) Leaf proteome analysis of eight *Populus* × *euramericana* genotypes: genetic variation in drought response and in water-use efficiency involves photosynthesis-related proteins. Proteomics 9:4121–4142

Brodribb T, Holbrook N, Edwards E, Gutierrez M (2003) Relations between stomatal closure, leaf turgor and xylem vulnerability in eight tropical dry forest trees. Plant Cell Environ 26:443–450

Chaves M, Oliveira M (2004) Mechanisms underlying plant resilience to water deficits: prospects for water-saving agriculture. J Exp Bot 55:2365–2384

Chaves MM, Pereira JS, Maroco J, Rodrigues ML, Ricardo CPP, Osorio ML, Carvalho I, Faria T, Pinheiro C (2002) How plants cope with water stress in the field. photosynthesis and growth. Ann Bot 89:907–916

Finazzi G, Rappaport F, Furia A, Fleischmann M, Rochaix JD, Zito F, Forti G (2002) Involvement of state transitions in the switch between linear and cyclic electron flow in *Chlamydomonas reinhardtii*. EMBO Rep 3:280–285

Fulda S, Mikkat S, Stegmann H, Horn R (2011) Physiology and proteomics of drought stress acclimation in sunflower (*Helianthus annuus* L.). Plant Biol 13:632–642

Gill SS, Tuteja N (2010) Reactive oxygen species and antioxidant machinery in abiotic stress tolerance in crop plants. Plant Physiol Biochem 48:909–930

Golldack D, Li C, Mohan H, Probst N (2014) Tolerance to drought and salt stress in plants: unraveling the signaling networks. Front Plant Sci 5:151

Hajheidari M, Abdollahian-Noghabi M, Askari H, Heidari M, Sadeghian SY, Ober ES, Hosseini Salekdeh G (2005) Proteome analysis of sugar beet leaves under drought stress. Proteomics 5:950–960

Hao GY, Sack L, Wang AY, Cao KF, Goldstein G (2010) Differentiation of leaf water flux and drought tolerance traits in hemiepiphytic and non-hemiepiphytic Ficus tree species. Funct Ecol 24:731–740

Hossain MM, Kant R, Van PT, Winarto B, Zeng S, Teixeira da Silva JA (2013) The application of biotechnology to orchids. Crit Rev Plant Sci 32:69–139

Huang W, Fu P-L, Jiang YJ, Zhang JL, Zhang SB, Hu H, Cao KF (2013) Differences in the responses of photosystem I and photosystem II of three tree species *Cleistanthus sumatranus*, *Celtis philippensis* and *Pistacia weinmannifolia* exposed to a prolonged drought in a tropical limestone forest. Tree Physiol 33:e220

Iwai M, Takizawa K, Tokutsu R, Okamuro A, Takahashi Y, Minagawa J (2010) Isolation of the elusive supercomplex that drives cyclic electron flow in photosynthesis. Nature 464:1210–1213

James HE, Bartling D, Musgrove J, Kirwin P, Herrmann R, Robinson C (1989) Transport of proteins into chloroplasts. Import and maturation of precursors to the 33-, 23-, and 16-kDa proteins of the photosynthetic oxygen-evolving complex. J Biol Chem 264:19573–19576

Jiang M, Zhang J (2001) Effect of abscisic acid on active oxygen species, antioxidative defence system and oxidative damage in leaves of maize seedlings. Plant Cell Physiol 42:1265–1273

Klein T (2014) The variability of stomatal sensitivity to leaf water potential across tree species indicates a continuum between isohydric and anisohydric behaviours. Funct Ecol 28:1313–1320

Kozlowski T, Pallardy S (2002) Acclimation and adaptive responses of woody plants to environmental stresses. Bot Rev 68:270–334

Kramer DM, Johnson G, Kiirats O, Edwards GE (2004) New fluorescence parameters for the determination of Q_A redox state and excitation energy fluxes. Photosynth Res 79:209–218

Kruger NJ (1994) The Bradford method for protein quantitation. Methods Mol Biol 32:9–15

Kuang M, Zhang SB (2015) Physiological response to high light in *Cymbidium tracyanum* and *C.sinense*. Plant Divers Resour 37:55–62

Lehtimäki N, Lintala M, Allahverdiyeva Y, Aro EM, Mulo P (2010) Drought stress-induced upregulation of components involved in ferredoxin-dependent cyclic electron transfer. J Plant Physiol 167:1018–1022

Li JW, Zhang SB (2016) Differences in the responses of photosystems I and II in *Cymbidium sinense* and *C. tracyanum* to long-term chilling stress. Front Plant Sci 6:1097

Li MH, Xiao WF, Shi P, Wang SG, Zhong YD, Liu XL, Wang XD, Cai XH, Shi ZM (2008) Nitrogen and carbon source-sink relationships in trees at the Himalayan treelines compared with lower elevations. Plant Cell Environ 31:1377–1387

Li X, Yang Y, Sun X, Lin H, Chen J, Ren J, Hu X, Yang Y (2014) Comparative physiological and proteomic analyses of poplar (*Populus yunnanensis*) plantlets exposed to high temperature and drought. PLoS One 9:e107605

Liu Z, Chen L, Liu K, Li L, Zhang Y, Huang L (2009) Climate warming brings about extinction tendency in wild population of *Cymbidium sinense*. Acta Ecol Sin 29:3443–3455

Luo Y, Jia J, Wang C (2002) A general review of the conservation status of Chinese orchids. Chin Biodivers 11:70–77

Manavalan LP, Guttikonda SK, Tran LSP, Nguyen HT (2009) Physiological and molecular approaches to improve drought resistance in soybean. Plant Cell Physiol 50:1260–1276

McDowell NG (2011) Mechanisms linking drought, hydraulics, carbon metabolism, and vegetation mortality. Plant Physiol 155:1051–1059

McDowell N, Pockman WT, Allen CD, Breshears DD, Cobb N, Kolb T, Plaut J, Sperry J, West A, Williams DG (2008) Mechanisms of plant survival and mortality during drought: why do some plants survive while others succumb to drought? New Phytol 178:719–739

Mittler R, Blumwald E (2015) The roles of ROS and ABA in systemic acquired acclimation. Plant Cell 27:64–70

Miyake C, Horiguchi S, Makino A, Shinzaki Y, Yamamoto H, Tomizawa K (2005) Effects of light intensity on cyclic electron flow around PSI and its relationship to non-photochemical quenching of Chl fluorescence in tobacco leaves. Plant Cell Physiol 46:1819–1830

Motomura H, Yukawa T, Ueno O, Kagawa A (2008) The occurrence of crassulacean acid metabolism in *Cymbidium* (Orchidaceae) and its ecological and evolutionary implications. J Plant Res 121:163–177

Nakano Y, Asada K (1981) Hydrogen peroxide is scavenged by ascorbate-specific peroxidase in spinach chloroplasts. Plant Cell Physiol 22:867–880

Nishiyama Y, Allakhverdiev SI, Murata N (2006) A new paradigm for the action of reactive oxygen species in the photoinhibition of photosystem II. Biochim et Biophys Acta-Bioenerg 1757:742–749

Noctor G, Foyer CH (1998) Ascorbate and glutathione: keeping active oxygen under control. Annu Rev Plant Biol 49:249–279

Ogburn R, Edwards EJ (2012) Quantifying succulence: a rapid, physiologically meaningful metric of plant water storage. Plant Cell Environ 35:1533–1542

Ohnishi N, Allakhverdiev SI, Takahashi S, Higashi S, Watanabe M, Nishiyama Y, Murata N (2005) Two-step mechanism of photodamage to photosystem II: step 1 occurs at the oxygen-evolving complex and step 2 occurs at the photochemical reaction center. Biochemistry 44:8494–8499

Pan R, Zheng X, Wen Z (1993) Change of water physiology of *Cymbidium sinense* during soil drought period. Acta Bot Yunnanica 16:379–384

Pinheiro C, Chaves MM, Ricardo CP (2001) Alterations in carbon and nitrogen metabolism induced by water deficit in the stems and leaves of *Lupinus albus* L. J Exp Bot 52:1063–1070

Porembski S, Barthlott W (1988) Velamen radicum micromorphology and classification of Orchidaceae. Nord J Bot 8:117–137

Price AH, Cairns JE, Horton P, Jones HG, Griffiths H (2002) Linking drought-resistance mechanisms to drought avoidance in upland rice using a QTL approach: progress and new opportunities to integrate stomatal and mesophyll responses. J Exp Bot 53:989–1004

Ramel F, Sulmon C, Gouesbet G, Couée I (2009) Natural variation reveals relationships between pre-stress carbohydrate nutritional status and subsequent responses to xenobiotic and oxidative stress in *Arabidopsis thaliana*. Ann Bot 104:1323–1337

Reddy AR, Chaitanya KV, Vivekanandan M (2004) Drought-induced responses of photosynthesis and antioxidant metabolism in higher plants. J Plant Physiol 161:1189–1202

Riemann M, Dhakarey R, Hazman M, Miro B, Kohli A (2015) Exploring jasmonates in the hormonal network of drought and salinity responses. Front Plant Sci 6:1077

Sakamoto W, Tamura T, Hanba-Tomita Y, Murata M (2002) The *VAR1* locus of *Arabidopsis* encodes a chloroplastic FtsH and is responsible for leaf variegation in the mutant alleles. Genes Cells 7:769–780

Seifter S, Dayton S, Novic B, Muntwyler E (1949) The estimation of glycogen with the anthrone reagent. Biochemistry 25:191–220

Shin M, Arnon DI (1965) Enzymic mechanisms of pyridine nucleotide reduction in chloroplasts. J Biol Chem 240:1405–1411

Shinozaki K, Yamaguchi-Shinozaki K (2007) Gene networks involved in drought stress response and tolerance. J Exp Bot 58:221–227

Spreitzer RJ, Salvucci ME (2002) Rubisco: structure, regulatory interactions, and possibilities for a better enzyme. Annu Rev Plant Biol 53:449–475

Suhita D, Raghavendra AS, Kwak JM, Vavasseur A (2004) Cytoplasmic alkalization precedes reactive oxygen species production during methyl jasmonate-and abscisic acid-induced stomatal closure. Plant Physiol 134:1536–1545

Takahashi S, Murata N (2008) How do environmental stresses accelerate photoinhibition? Trends Plant Sci 13:178–182

Takahashi S, Bauwe H, Badger M (2007) Impairment of the photorespiratory pathway accelerates photoinhibition of photosystem II by suppression of repair but not acceleration of damage processes in *Arabidopsis*. Plant Physiol 144:487–494

Tardieu F, Simonneau T (1998) Variability among species of stomatal control under fluctuating soil water status and evaporative demand: modelling isohydric and anisohydric behaviours. J Exp Bot 49:419–432

Théry M (2001) Forest light and its influence on habitat selection. In: Linsenmair KE, Davis AJ, Fiala B, Speight MR (eds) Tropical forest canopies: ecology and management. Springer, Dordrecht, pp 251–261

Tikkanen M, Mekala NR, Aro E-M (2014) Photosystem II photoinhibition-repair cycle protects photosystem I from irreversible damage. Biochim et Biophys Acta -Bioenerg 1837:210–215

Tyree M, Hammel H (1972) The measurement of the turgor pressure and the water relations of plants by the pressure-bomb technique. J Exp Bot 23:267–282

Vallon O, Bulte L, Dainese P, Olive J, Bassi R, Wollman F-A (1991) Lateral redistribution of cytochrome b6/f complexes along thylakoid membranes upon state transitions. Proc Natl Acad Sci 88:8262–8266

Wilkinson S, Kudoyarova GR, Veselov DS, Arkhipova TN, Davies WJ (2012) Plant hormone interactions: innovative targets for crop breeding and management. J Exp Bot 63:3499–3509

Yang Y, Chen J, Liu Q, Ben CC, Todd CD, Shi J, Yang Y, Hu X (2012) Comparative proteomic analysis of the thermotolerant plant *Portulaca oleracea* acclimation to combined high temperature and humidity stress. J Proteome Res 11:3605–3623

Yordanov I, Velikova V, Tsonev T (2000) Plant responses to drought, acclimation, and stress tolerance. Photosynthetica 38:171–186

Yoshioka M, Uchida S, Mori H, Komayama K, Ohira S, Morita N, Nakanishi T, Yamamoto Y (2006) Quality control of photosystem II cleavage of reaction center D1 protein in spinach thylakoids by FtsH protease under moderate heat stress. J Biol Chem 281:21660–21669

Youssef A, Laizet Yh, Block MA, Maréchal E, Alcaraz JP, Larson TR, Pontier D, Gaffé J, Kuntz M (2010) Plant lipid-associated fibrillin proteins condition jasmonate production under photosynthetic stress. Plant J 61:436–445

Yukawa T, Stern WL (2002) Comparative vegetative anatomy and systematics of *Cymbidium* (Cymbidieae: Orchidaceae). Bot J Linn Soc 138:383–419

Zhang M, Sun C, Hao G, Ye X, Liang C, Zhu G (2001) A preliminary analysis of phylogenetic relationships in *Cymbidium* (Orchidaceae) based on nrITS sequence data. Acta Bot Sin 44:588–592

Zhang SB, Dai Y, Hao GY, Li JW, Fu XW, Zhang JL (2015) Differentiation of water-related traits in terrestrial and epiphytic *Cymbidium* species. Front Plant Sci 6:260

Zhang W, Hu H, Zhang SB (2016) Divergent adaptive strategies by two co-occurring epiphytic orchids to water stress: escape or avoidance? Front Plant Sci 7:588

Zotz G, Bader M (2009) Epiphytic plants in a changing world: global change effects on vascular and non-vascular epiphytes. In: Canovas FM, Luttge U, Matyssek R (eds) Progress in botany. Springer, Dordrecht, pp 147–170

Zotz G, Hietz P (2001) The physiological ecology of vascular epiphytes: current knowledge, open questions. J Exp Bot 52:2067–2078

Zotz G, Tyree MT (1996) Water stress in the epiphytic orchid, *Dimerandra emarginata* (G. Meyer) Hoehne. Oecologia 107:151–159

Zotz G, Winkler U (2013) Aerial roots of epiphytic orchids: the velamen radicum and its role in water and nutrient uptake. Oecologia 171:733–741